A

Dissertation Report on

"Synthesis and Characterization of Graphene based hydroxyapatite nanocomposite by hydrothermal method for its biomedical application.

Submitted

In partial fulfillment of the requirements for the degree of

Master of Technology

In

Design Engineering

by

Mr. Suyog Balavant Sutar (2321007)

Under the Guidance of

Dr. Santosh. R. Patil

Mechanical Engineering Department

K. E. Society's

Rajarambapu Institute of Technology, Rajaramnagar

(An Autonomous Institute, Affiliated to Shivaji University, Kolhapur)

2024 - 2025

ACKNOWLEDGEMENT

We take this opportunity to thank all those who have contributed in the successful completion of project work entitle **"Synthesis and Characterization of Graphene based hydroxyapatite nanocomposite by Hydrothermal method for its biomedical application"**. We sincerely wish to express our gratitude to Project supervisor Prof. S. R. Patil for full support, expert guidance, encouragement, and kind cooperation throughout the project work. We are greatly indebted to him for his help throughout project work. We express our sincere gratitude towards Dr. R. M. Kurane, Head of the Department, Mechanical Engineering, for providing necessary facilities, guidance, and support.

We are thankful to and fortunate enough to get constant encouragement, support and guidance from all Teaching staffs of Mechanical Engineering Department, which helped us in successfully completing our project work. Also, we would like to extend our sincere esteems to all staff in the laboratory for their timely support. Nevertheless, we express our gratitude toward our families and colleagues for their kind co-operation and encouragement which help us in the completion of this project.

ABSTRACT

The research focuses on the development of an artificial human bone using a nanocomposite material composed of hydroxyapatite (nHA), polymethyl methacrylate (PMMA), and zirconia (ZrO_2). The synthesis of the nanocomposite was carried out using powder metallurgy techniques, which involve the blending of fine powdered materials, compacting them into a desired shape, and then heating them to bond the particles. This method allows for precise control over the material's composition and microstructure.

The mechanical, structural, and biocompatibility properties of the resulting nanocomposite were thoroughly characterized. Mechanical testing revealed that the nanocomposite exhibits properties closely matching those of natural human bone, including high strength and stiffness, which are crucial for its use in load-bearing applications. Structural analysis showed that the nanocomposite has a well-organized microstructure that mimics the hierarchical architecture of natural bone, providing an ideal environment for bone cell attachment and growth.

Biocompatibility studies indicated that the nanocomposite is non-toxic and supports the proliferation and differentiation of osteoblasts (bone-forming cells), which are essential for effective bone regeneration. The incorporation of hydroxyapatite, a naturally occurring mineral in bone, enhances the bioactivity of the material, while polymethyl methacrylate provides flexibility and toughness. Zirconia contributes to the overall mechanical strength and stability of the nanocomposite.

These findings suggest that the developed nanocomposite is a promising material for bone repair and replacement applications. Its combination of biocompatibility, mechanical properties, and structural similarity to natural bone makes it a suitable candidate for use in orthopedic implants and other bone-related medical devices.

TABLE OF CONTENTS

CHAPTER 1: INTRODUCTION.....6

1.1 Background.....6

1.2 Motivation of Present Work.....7

1.3 Problem Statement.....7

1.4 Objectives.....8

1.5 Scope and Limitations.....8

CHAPTER 2: LITERATURE REVIEW.....9

2.1 Introduction.....9

2.2 Research.....9

2.3 Research Gap.....12

CHAPTER 3: METHODOLOGY FOR NANOCOMPOSITE PREPARATION.....13

3.1 Preparation of Graphene Oxide (GO).....13

3.2 Preparation of Hydroxyapatite (HA) Precursor.....13

3.3 Synthesis of Graphene-Based HA Nanocomposite.....14

3.4 Characterization of the Nanocomposite.....14

3.5 Preparation of Solution in our Chemistry Lab.....15

3.6 Final Product.....17

CHAPTER 4: CHEMICAL AND STRUCTURAL CHARACTERIZATION.....18

4.1 Fourier Transform Infrared (FTIR) Spectroscopy.....18

4.2 FTIR of n-hydroxyapatite sample.....20

4.3 FTIR of n-hydroxyapatite-graphene-ferrocene composite sample.....21

4.4 X-ray Diffraction (XRD).....22

4.5 Transmission Electron Microscopy (TEM).....26

4.6 Energy-Dispersive X-ray Spectroscopy (EDX).....30

4.7 Raman Spectroscopy.....34

4.8 Thermogravimetric Analysis/Differential Thermal Analysis (TGA/DTA)...38

4.9 BET Surface Area Analysis.....44

CHAPTER 5: BIOCOMPATIBILITY AND CYTOTOXICITY ANALYSIS.....58

5.1 Biocompatibility Analysis.....58

CHAPTER 6: METHODOLOGY OF BONE PIN FORMATION USING POWDER METALLURGY.....61

6.1 Material Preparation.....61

6.2 Die Design and Setup.....62

6.3 Screw Specifications.....62

6.4 Compaction Process.....63

6.5 Bone Pin Ejection.....63

CHAPTER 7: MECHANICAL ANALYSIS.....65

7.1 Density Analysis.....65

7.2 Finite Element Analysis.....66

7.3 Tribological Analysis.....70

CHAPTER 8: RESULT ANALYSIS.....73

8.1 Chemical and Structural Result Analysis.....73

8.2 Biocompatibility and Cytotoxicity Result Analysis.....74

8.3 Mechanical Result Analysis.....75

CHAPTER 9: CONCLUSION AND FUTURE SCOPE.....77

9.1 Conclusion.....77

9.2 Future Scope.....78

REFERENCES.....80

LIST OF FIGURES

Figure 3.1: Chemical Process.....15

Figure 3.2: Elements Procedure.....16

Figure 3.3: Final Composition.....17

Figure 4.1: FTIR at Shivaji University Kolhapur.....19

Figure 4.2: FTIR spectrum for sample of nano hydroxyapatite.....20

Figure 4.3: FTIR spectrum for sample of composite.....21

Figure 4.4: XRD at Shivaji University Kolhapur.....24

Figure 4.5: XRD spectrum for composite.....25

Figure 4.6: TEM/EDX at Shivaji University Kolhapur.....31

Figure 4.7: TEM images of nano composite.....34

Figure 4.8: EDX of nanocomposite.....34

Figure 4.9-4.13: EDX mapping of elements in composite (C, O, P, Ca, Fe).....34

Figure 4.14: Raman Spectrometer at Shivaji University Kolhapur.....40

Figure 4.15: Raman spectroscopy graph of nano composite.....41

Figure 4.16: TGA/DTA at Shivaji University Kolhapur.....42

Figure 4.17: TGA graph of nano composite.....46

Figure 4.18: DTA graph of Nano composite.....47

Figure 4.19: Absolute Pressure vs Volume (BET).....48

Figure 4.20: Data on Log scale (BET).....49

Figure 4.21: Absolute Pressure vs Volume (BET).....50

Figure 4.22: Multi point BET plot.....51

Figure 4.23: Single point surface area.....51

Figure 4.24: Pore size distribution (adsorption).....52

Figure 4.25: Pore size distribution (desorption).....52

Figure 5.1: Graphical representation of biocompatibility at varying concentrations.60

Figure 6.1: Nano composite powder.....61

Figure 6.2: Die and pin setup.....62

Figure 6.3: Bone pin after removal from Die.....64

Figure 7.1: Extruded cylinder (FEA Model).....67

Figure 7.2: Meshed Cylinder.....67

Figure 7.3: Mesh with Boundary conditions applied.....68

Figure 7.4: Test setup for tribological testing.....70

Figure 7.5: Wear, Frictional Force and COF charts of tribological testing.....71

.

LIST OF TABLES

Table 4.1: Tabularized data of EDX analysis.....32

Table 4.2: Summary of BET analysis.....57

Table 5.1: Effect of nanocomposite against L929 cell lines.....59

1.Introduction

1.1 Background

Bone-related diseases, injuries, and age-related degeneration have created a growing demand for advanced biomaterials that can effectively repair or replace damaged bone tissue. Traditional treatments, such as autografts and allografts, face significant limitations, including donor site morbidity, risk of infection, immunological rejection, and limited availability of donor tissue. As a result, there is a critical need for innovative artificial bone substitutes that can closely mimic the natural structure, composition, and functionality of human bone while promoting regeneration and integration with the body.

In recent years, **nanocomposites** have emerged as a promising solution in bone tissue engineering due to their unique ability to combine the strengths of different materials. Among these, **hydroxyapatite (HA)**, a naturally occurring mineral in bones, has gained significant attention for its excellent biocompatibility, bioactivity, and ability to bond with bone tissue. However, pure hydroxyapatite often lacks the mechanical strength required for load-bearing applications. To address this, researchers have explored combining HA with other materials, such as **graphene**, a two-dimensional carbon-based material known for its exceptional mechanical strength, electrical conductivity, and biocompatibility.

The integration of graphene with hydroxyapatite offers a synergistic approach to developing nanocomposites with enhanced mechanical properties, bioactivity, and osteo conductivity. The **hydrothermal method**, a widely used synthesis technique, provides a controlled environment for creating such nanocomposites with precise structural and compositional properties. This method allows for the uniform distribution of graphene within the hydroxyapatite matrix, resulting in a material that closely mimics the hierarchical structure of natural bone.

This project focuses on the **synthesis and characterization of graphene-based hydroxyapatite nanocomposites** using the hydrothermal method. The goal is to develop a biomaterial with improved mechanical strength, biocompatibility, and bioactivity for potential biomedical applications, particularly in bone tissue engineering. By combining the

unique properties of graphene and hydroxyapatite, this study aims to create a nanocomposite that can serve as an effective artificial bone substitute, addressing the limitations of traditional treatments and offering a promising solution for bone repair and regeneration.

1.2 Motivation of present work

The development of advanced biomaterials for bone repair is a critical need in modern medicine, as traditional treatments like autografts and allografts face significant challenges such as limited availability, donor site morbidity, and risk of rejection. Graphene-based hydroxyapatite nanocomposites offer a groundbreaking solution by combining the exceptional mechanical strength of graphene with the biocompatibility and bioactivity of hydroxyapatite. This project aims to synthesize and characterize such nanocomposites using the hydrothermal method, paving the way for innovative biomedical applications in bone tissue engineering. By addressing the limitations of current treatments, this research holds the potential to revolutionize bone repair and regeneration, improving the quality of life for patients worldwide.

1.3 Problem Statement

Bone defects caused by trauma, disease, or age-related degeneration pose significant challenges in healthcare, as traditional treatments like autografts and allografts are limited by issues such as donor site morbidity, risk of infection, immunological rejection, and insufficient donor availability. While hydroxyapatite (HA) has shown promise as a biomaterial due to its biocompatibility and bioactivity, its poor mechanical strength restricts its use in load-bearing applications. To address these limitations, there is a pressing need to develop advanced nanocomposites that combine the strengths of HA with materials like graphene, which offers exceptional mechanical properties and biocompatibility. However, achieving a uniform and effective integration of graphene with HA remains a challenge. This project focuses on synthesizing and characterizing graphene-based hydroxyapatite nanocomposites using the hydrothermal method, aiming to create a biomaterial with enhanced mechanical strength, bioactivity, and osteo conductivity for use in bone tissue engineering. The success of this research could provide a viable alternative to traditional bone repair methods, overcoming their limitations and improving patient outcomes.

1.4 Objectives

1. To identify and select nanocomposite that exhibits the biocompatible properties.

2. To develop artificial bone pin using proposed nanocomposite material.

3. To synthesize nanocomposite by hydrothermal chemical method and characterize it.

4. To investigate mechanical properties of developed artificial bone pin by computational and experimental methods.

5. To check the biocompatibility of artificial bone pin material.

1.5 Scope and Limitations

This project focuses on synthesizing and characterizing graphene-based hydroxyapatite (HA) nanocomposites using the hydrothermal method for bone tissue engineering applications. The study aims to enhance the mechanical strength, bioactivity, and osteo conductivity of HA by integrating graphene, creating a biomaterial that mimics natural bone. The research will evaluate the structural and biocompatibility properties of the nanocomposite, offering a potential alternative to traditional bone repair methods.

1. **Material Integration**: Achieving uniform graphene-HA integration may be challenging due to differences in their properties.

2. **Scalability**: Scaling up production for clinical use could be technically and economically difficult.

3. **Testing**: Comprehensive biocompatibility and long-term performance testing may extend beyond this study.

4. **Mechanical Performance**: The nanocomposite may not fully replicate natural bone's strength in high-load applications.

5. **Regulatory and Cost Barriers**: Clinical translation requires extensive approvals, and production costs may limit accessibility.

2. Literature Review

2.1 Introduction

Bone loss and fractures of bone tissues are serious medical problems which await for the efficient bone reconstruction and repair techniques. The standard approaches, such as auto- or allografts, also have shortcomings among them are donor site complications as well as a lack of biological signaling2. The development of bioactive coatings for nanocomposite bone pins is a part of a new trend in biomedical technology that has great prospects for the improvement
of bone regeneration1.Nanocomposite bone pins are made to replicate the nanostructure of ECM to facilitate cell adhesion, proliferation and subsequent differentiation1. In general biopolymeric pins, hydroxyapatite (Hap) and graphene oxide (GO) as nanosized fillers are used to reinforce the mechanical properties and osteogenic activity of the pins. Their aim is to create a biocompatible and biodegradable scaffold which is essential for bone regeneration2.This review will analyze advances in the filed of nanocomposite bone pins in aspects of current design, composition, structure and application potentials in bone tissue engineering and regenerative medicine1. Within this context, the review will outline the limitations and new scope of research in order to put these materials into practice.

2.2 Research

Patil S. R. et al. [1]

Investigated synthesis of Hydroxyapatite Polymethyl methacrylate Zirconia (Hap-PMMA-ZrO2) composite by using powder metallurgy technique. They have characterize mechanical, morphological, in vitro biocompatibility and tribological properties were characterized by universal testing machine, micro vickers hardness tester, high resolution transmission electron microscope (HR TEM), MTT assay and pin on disc setup of novel biocomopsite material. Hap-PMMA-ZrO2 scaffold displayed good biocompatibility and other properties.

Andrea Papait [2]

Graphene oxide (GO) is a promising nanomaterial for biomedical applications like bioimaging and drug delivery. This study explores how GO affects immune cell function when integrated into PLGA scaffolds. High GO levels reduce the viability of PBMCs and impair T cell activation and differentiation. GO minimally impacts resting monocytes but

significantly affects monocyte maturation into M1 and M2 macrophages. This research highlights the importance of optimizing GO-to-PLGA ratios for safe biomaterial design, addressing concerns about immune responses and advancing GO-based clinical applications.

Shanmuga Priya Mohanaraman [3]

Graphene quantum dots (GQDs) are carbon nanomaterials known for their optical properties, engineered structures, and photostability. They are biocompatible, low in toxicity, hydrophilic, and have functionalized surfaces suitable for biological applications. GQDs emit various colors under UV light, with red light offering deep tissue penetration, cell imaging, and drug delivery benefits, making them ideal for photodynamic therapy. This review covers synthesis methods for red fluorescence GQDs (RF-GQDs), analyzes spectral characterization techniques, examines red emission mechanisms, and explores their biological applications and challenges, highlighting potential clinical and industrial uses.

Zobia Ayreen [4]

Advancements in nanotechnology have highlighted the potential of graphene oxide nanoparticles (GONP) due to their unique properties, but concerns about their immunotoxic effects have emerged. This review examines their interactions with biological systems, including human blood, immune cells, cancer cell lines, and in vivo models like mice and zebrafish, revealing effects such as inflammation, immunosuppression, hypersensitivity, and cytotoxicity. It provides insights for researchers and policymakers to harness GONP's benefits while addressing health and environmental risks.

Rebecca Goodrum [5]

Graphene's exceptional properties, such as high conductivity and elasticity, make it ideal for biomedical applications like biosensing and drug delivery. This review highlights recent advances in green synthesis of graphene-based nanomaterials, focusing on top-down and bottom-up approaches. Applications in optical and electrochemical biosensors are explored, emphasizing their enhanced sensitivity for detecting biomolecules and cells. The benefits, challenges, and future directions of graphene-based biosensors are summarized, comparing their performance with conventional techniques.

Safeena Zafar [6]

Antimicrobial resistance necessitates new agents to protect health. Graphene and its derivatives, decorated with inorganic nanoparticles like FeO/NiO, show promising antibacterial and antifungal properties. Synthesized via a wet chemical method, these nanocomposites were analyzed using XRD, IR, SEM, and more. FeO/NiO/N-GO showed moderate antibacterial activity (MIC: 12.5 μg/mL), while FeO/NiO and FeO/NiO/S-GO exhibited strong antifungal effects. Their antioxidant, cytotoxic, and hemolytic potentials were also evaluated, with all showing significant activity. These findings support their potential in pharmaceutical and biomedical applications.

Shramila Yadav [7]

To promote sustainability, advanced systems with controlled performance are essential for biomedical, environmental, and energy applications. While graphene-based nanomaterials are well-studied, emerging 2D materials like TMDs, TMOs, MXenes, Xenes, and MOFs remain underexplored for next-gen biomedical uses. This review critically examines their roles in drug delivery, cancer therapy, tissue engineering, and biosensing, highlighting the need for better control over their shape, size, and properties. It fills a gap in the literature by providing a comprehensive analysis of these materials, offering valuable insights for researchers aiming to develop adaptable, high-performance 2D material-based applications.

2.3 Research Gap

Despite the promising potential of hydroxyapatite (HA) in bone tissue engineering, its poor mechanical strength limits its use in load-bearing applications. While graphene has been recognized for its exceptional mechanical properties and biocompatibility, its integration with HA to create a robust nanocomposite remains underexplored. Existing studies often lack a systematic approach to optimizing the synthesis process, particularly using the hydrothermal method, to achieve a uniform and stable graphene-HA structure. Additionally, there is limited research on the comprehensive characterization of such nanocomposites, including their mechanical properties, bioactivity, and biocompatibility, to ensure their suitability for biomedical applications. This project addresses these gaps by focusing on the development and detailed evaluation of graphene-based HA nanocomposites, aiming to create a material that overcomes the limitations of traditional bone repair methods and offers a viable alternative for bone regeneration.

3. Methodology for nanocomposite preparation

The synthesis of graphene-based hydroxyapatite (HA) nanocomposites involves a series of well-defined steps to ensure the uniform integration of graphene with hydroxyapatite, resulting in a material with enhanced mechanical and biological properties. Below is a detailed explanation of the synthesis process:

3.1. Preparation of Graphene Oxide (GO)

- **Materials**: Graphite powder, sulfuric acid (H_2SO_4), phosphoric acid (H_3PO_4), potassium permanganate ($KMnO_4$), hydrogen peroxide (H_2O_2), and deionized water.
- **Procedure**:
    1. **Oxidation of Graphite**: Graphite powder is oxidized using a modified Hummers' method. This involves mixing graphite with concentrated H_2SO_4 and H_3PO_4 in a controlled ratio, followed by the gradual addition of $KMnO_4$ under constant stirring and cooling to prevent overheating.
    2. **Reaction and Dilution**: The mixture is stirred for several hours to ensure complete oxidation. Deionized water is then added slowly, causing an exothermic reaction. The mixture is further treated with H_2O_2 to terminate the reaction, resulting in a bright yellow solution.
    3. **Purification**: The graphene oxide (GO) is washed repeatedly with deionized water and hydrochloric acid (HCl) to remove impurities, followed by centrifugation and drying to obtain GO powder.

3.2. Preparation of Hydroxyapatite (HA) Precursor

- **Materials**: Calcium nitrate tetrahydrate ($Ca(NO_3)_2 \cdot 4H_2O$), ammonium dihydrogen phosphate ($NH_4H_2PO_4$), and ammonia solution (NH_4OH).
- **Procedure**:
    1. **Solution Preparation**: Aqueous solutions of calcium nitrate and ammonium dihydrogen phosphate are prepared separately in stoichiometric ratios to ensure a Ca/P ratio of 1.67, matching natural bone.

2. **Mixing and pH Adjustment**: The two solutions are mixed under constant stirring, and the pH is adjusted to 10–11 using ammonia solution to promote the formation of HA.
3. **Aging**: The mixture is aged for 24 hours at room temperature to allow the formation of HA nanoparticles.

3.3. Synthesis of Graphene-Based HA Nanocomposite

- **Materials**: Graphene oxide (GO), HA precursor, and deionized water.
- **Procedure**:
    1. **Dispersion of GO**: Graphene oxide is dispersed in deionized water using ultrasonication to achieve a homogeneous suspension.
    2. **Mixing with HA Precursor**: The HA precursor solution is added to the GO suspension under continuous stirring to ensure uniform mixing.
    3. **Hydrothermal Treatment**: The mixture is transferred to a Teflon-lined autoclave and subjected to hydrothermal treatment at 120–180°C for 12–24 hours. This step promotes the reduction of GO to reduced graphene oxide (rGO) and the crystallization of HA, resulting in a well-integrated graphene-HA nanocomposite.
    4. **Cooling and Washing**: After hydrothermal treatment, the autoclave is cooled to room temperature, and the resulting nanocomposite is washed repeatedly with deionized water and ethanol to remove unreacted impurities.
    5. **Drying**: The final product is dried in an oven at 60–80°C to obtain the graphene-based HA nanocomposite powder.

3.4. Characterization of the Nanocomposite

- **Structural Analysis**: Techniques like X-ray diffraction (XRD) and Fourier-transform infrared spectroscopy (FTIR) are used to confirm the formation of HA and the presence of graphene.
- **Morphological Analysis**: Scanning electron microscopy (SEM) and transmission electron microscopy (TEM) are employed to study the surface morphology and distribution of graphene within the HA matrix.
- **Mechanical Testing**: The mechanical properties, such as compressive strength and elasticity, are evaluated using universal testing machines.

- **Biocompatibility Testing**: In vitro studies are conducted to assess cell viability, proliferation, and differentiation on the nanocomposite surface.

3.5 Preparation of Solution in our Chemistry Lab

Below is the detailed and properly structured procedure for the synthesis of the graphene-based hydroxyapatite nanocomposite as carried out in the lab:

- **Materials Required**

1. Calcium Nitrate ($Ca(NO_3)_2$) – 14.16 gm
2. Ammonia Solution (NH_4OH) – 15 ml
3. Ammonium Hydrogen Phosphate ($(NH_4)_2HPO_4$) – 4.74 gm
4. Graphene ($(CH)_n$) – 0.1 gm
5. Ferrocene ($C_{10}H_{10}Fe$) – 0.5 gm
6. Zirconium Dioxide (ZrO_2) – 3.5 gm
7. Distilled Water (H_2O) – 300 ml
8. Ethyl Acetate ($C_4H_8O_2$) – As needed
9. Diethyl Ether – As needed

Step 1: Preparation of Solution A

1. Take a round-bottom flask and add **14.16 gm of Calcium Nitrate ($Ca(NO_3)_2$)** and **150 ml of Distilled Water (H_2O)**.
2. Mix the solution well using a glass rod to ensure complete dissolution.
3. Place the flask on a magnetic stirrer and add **15 ml of Ammonia Solution (NH_4OH)**.
4. Stir the solution for about 10 minutes to ensure proper mixing.
5. Keep the magnetic stirrer running for the next steps.

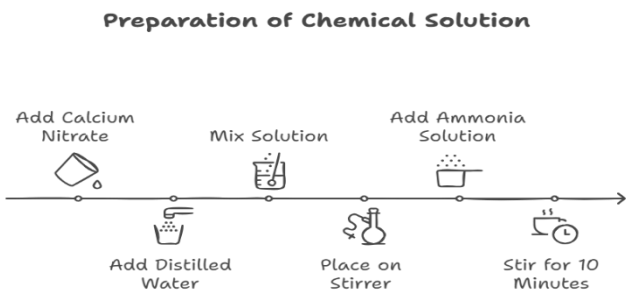

Figure 3.1- Chemical Process

Step 2: Preparation of Solution B (Graphene Suspension)

1. Take a beaker and add the following materials:
    - **0.1 gm of Graphene ($(CH)_n$)**
    - **0.5 gm of Ferrocene ($C_{10}H_{10}Fe$)**
    - **3.5 gm of Zirconium Dioxide (ZrO_2)**
    - **4.74 gm of Ammonium Hydrogen Phosphate ($(NH_4)_2HPO_4$)**
    - **100 ml of Distilled Water (H_2O)**
2. Use an ultrasonic cleaner (sonicator) to mix the solution for **50 minutes**. Ensure the mixture is homogeneous by mixing it repeatedly during the process.

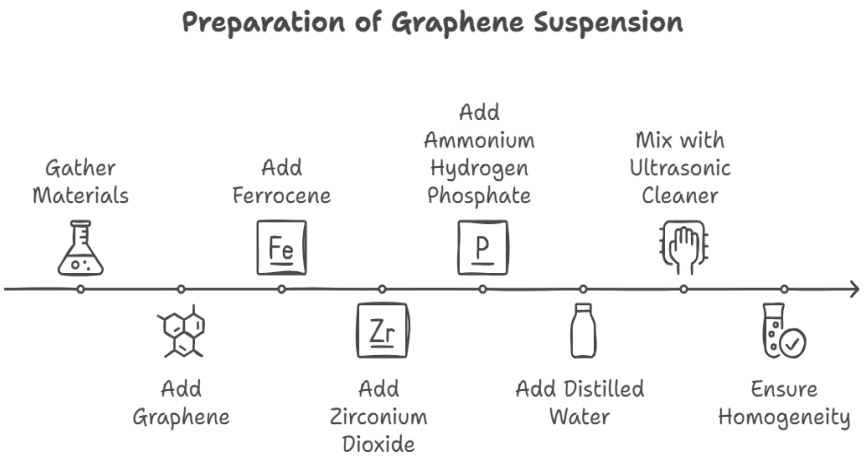

Figure 3.2- Elements Procedure

Step 3: Mixing Solutions A and B

1. Gradually add **Solution B** (graphene suspension) into **Solution A** in small amounts while stirring continuously.
2. Allow the mixing process to continue for about **10 minutes** to ensure a uniform mixture.
3. After combining the two solutions, keep the magnetic stirrer running for **18 hours** to ensure thorough mixing and reaction.

Step 4: Heating the Solution

1. Transfer the mixed solution to a heating mantle.

2. Heat the solution at a temperature of **60°C** for **4 hours** while maintaining continuous stirring.

Step 5: Filtration

1. Set up a vacuum filtration system with a filter paper placed in a funnel.
2. Filter the heated solution using the vacuum filtration setup.
3. Stop the filtration process once the solution attains a mud-like consistency.
4. Transfer the filtered material to a bowl.

Step 6: Drying and Crushing

1. Place the bowl on a gas stove and heat it at a **low flame** until the material forms hard lumps.
2. Once the lumps are formed, crush them into a fine powder using a mortar and pestle or a similar tool.

Step 7: Calcination

1. Transfer the powdered material to a heat-resistant bowl.
2. Place the bowl in a muffle furnace and heat it at **350°C** for **4 hours**.
3. After the calcination process is complete, allow the furnace to cool down to room temperature before removing the bowl.

3.6 Final Product

The resulting material is a graphene-based hydroxyapatite nanocomposite in powder form, ready for further characterization and testing for biomedical applications.

This procedure ensures the synthesis of a uniform and well-integrated nanocomposite with enhanced mechanical and biological properties, suitable for bone tissue engineering applications.

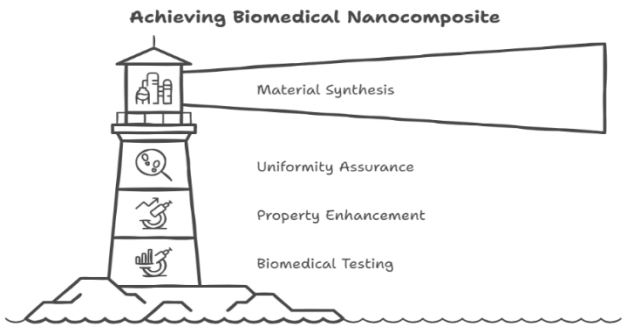

Figure 3.3- Final Composition

4. Chemical and Structural Characterization

4.1. Fourier Transform Infrared (FTIR) Spectroscopy: -

FTIR is Fourier Transform Infrared Spectroscopy, a powerful analytical tool used in a variety of scientific and industrial fields to investigate the molecular structure and composition of materials. It is an analytical technique used to identify the chemical composition and structure of a sample. It works by measuring how a sample absorbs infrared radiation at different wavelengths.

FTIR spectroscopy is based on the principle of how different chemical bonds in a molecule absorb infrared radiation at characteristic frequencies; the absorption is related to the vibrational modes of the atoms in the molecule. By measuring the absorption of these frequencies, it gives information about the functional groups and overall structure of the molecule.

When infrared light passes through or reflects off a sample, the bonds between atoms in the molecules can vibrate in different ways, such as:

•***Stretching:*** The length of the bond changes (e.g., C-H stretching, O-H stretching).

•***Bending:*** The angle between bonds changes (e.g., bending vibrations in water).

•***Twisting and Rocking***: The molecule moves in more complex ways.

Each variety of vibration absorbs infrared light at certain frequencies that result in the unique absorption pattern, or spectrum.

o FTIR Working Process:

1. ***Source of Infrared Radiation***: The FTIR spectrometer emits infrared light in a range of wavelengths.

2. Interaction with Sample: Some of the infrared radiation is absorbed by the sample, while the remaining passes through or gets reflected.

3. Interferometer: The interferometer in a spectrometer modulates the infrared light, thereby producing an interferogram which is a type of signal that holds information on the absorptivity features of the sample.

4. Fourier Transform: The interferogram is then mathematically treated as a Fourier transform to convert the obtained data into an absorption spectrum, which reflects the quantity of absorption of infrared radiation by the sample at each wavelength.

5. Spectrum Analysis: The resulting spectrum shows peaks that correspond to specific vibrational frequencies of the chemical bonds in the molecules of the sample. These peaks can be used to identify functional groups and molecular structures.

The absorption spectrum obtained is a plot of absorbance or sometimes transmittance against wavenumber expressed in cm^{-1}. Each peak in the spectrum corresponds to an absorption at a specific wavenumber and reflects the vibrational frequency of the molecular bonds in the sample.

The main features of the spectrum include:

•***Fingerprint Region:*** Generally, between 1500 cm^{-1} and 500 cm^{-1}. This region is unique for each substance, and used for accurate identification of compounds.

•***Functional Group Region:*** Typically, between 4000 cm^{-1} and 1500 cm^{-1}. Strong peaks are generally attributed to more common functional groups, such as -OH, -NH, -CH, and C=O.

Figure 4.1- FTIR at Shivaji University Kolhapur.

Chemical composition and molecular structure identification samples were carried out using Fourier Transform Infrared (FTIR) spectroscopy at Shivaji University, Kolhapur. The analysis was carried out using the JASCO FT/IR-4700 high-precision and advanced spectrometer manufactured by JASCO, Japan. It is a high-performance reliability model with a spectral range of 4000-350 cm^{-1} thus enabling broad mid-infrared and far infrared range. The JASCO FT/IR-4700 can provide a resolution up to 0.5 cm^{-1} that enables the accurate identification of minute absorption peaks that correspond to various molecular vibrations.

4.2 FTIR of n-hydroxyapatite sample-

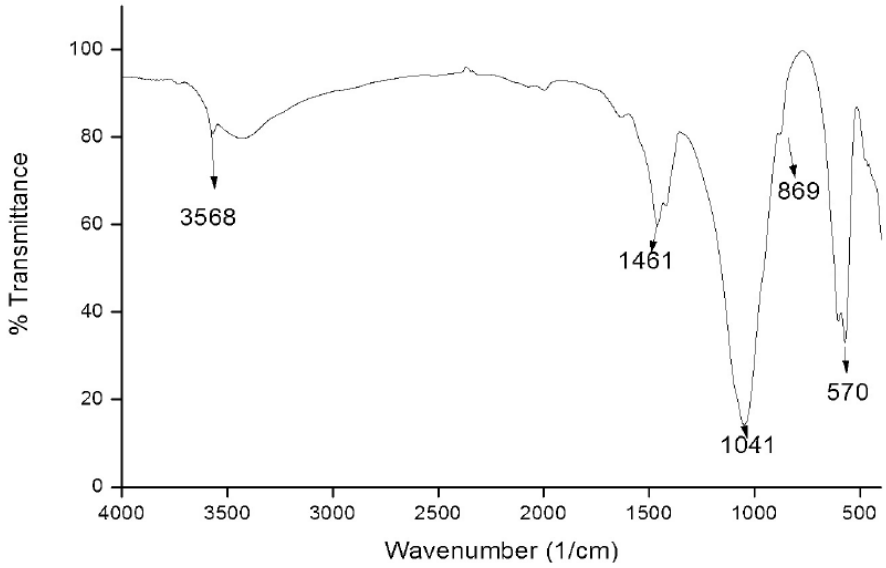

Figure 4.2: FTIR spectrum for sample of nano hydroxyapatite

Based on the FTIR spectrum above we can analyze that-

1. O-H Stretching Vibration (3568 cm^{-1}):

A prominent broad peak observed at 3568 cm^{-1} is characteristic of O-H stretching vibrations, confirming the presence of hydroxyl (OH^-) groups. This peak is primarily associated with hydroxyapatite, indicating its successful incorporation into the composite.

2. Carbonate Substitution (1461 and 869 cm^{-1}):

The presence of peaks at 1461 cm^{-1} and 869 cm^{-1} is indicative of carbonate (CO_3^{2-}) substitution. These peaks correspond to the stretching and out-of-plane bending vibrations of carbonate groups, respectively. While minor carbonate substitution is common during the synthesis or handling of hydroxyapatite, it can enhance the biocompatibility of the material by increasing its similarity to natural bone mineral.

3. Phosphate Group Vibrations (1041 and 570 cm^{-1}):

The intense band at 1041 cm^{-1} is attributed to the asymmetric stretching vibrations of phosphate (PO_4^{3-}) groups, confirming the primary structural component of hydroxyapatite. Additionally, the peak at 570 cm^{-1} corresponds to the bending vibrations of phosphate groups, further supporting the presence of hydroxyapatite in the composite.

The FTIR spectrum of the sample was analyzed to confirm the structural integrity and composition of the synthesized nano-hydroxyapatite. Key observations include:

These results confirm the successful synthesis of pure hydroxyapatite. The observed carbonate peaks (1461 and 869 cm^{-1}) likely arise from secondary carbonate substitution, which is a common occurrence during the synthesis or handling of hydroxyapatite under atmospheric conditions. Such substitution enhances the similarity of the material to natural bone mineral and contributes to its excellent biocompatibility, making it highly suitable for biomedical applications such as bone repair and regeneration.

4.3 FTIR of n-hydroxyapatite-graphene-ferrocene composite sample-

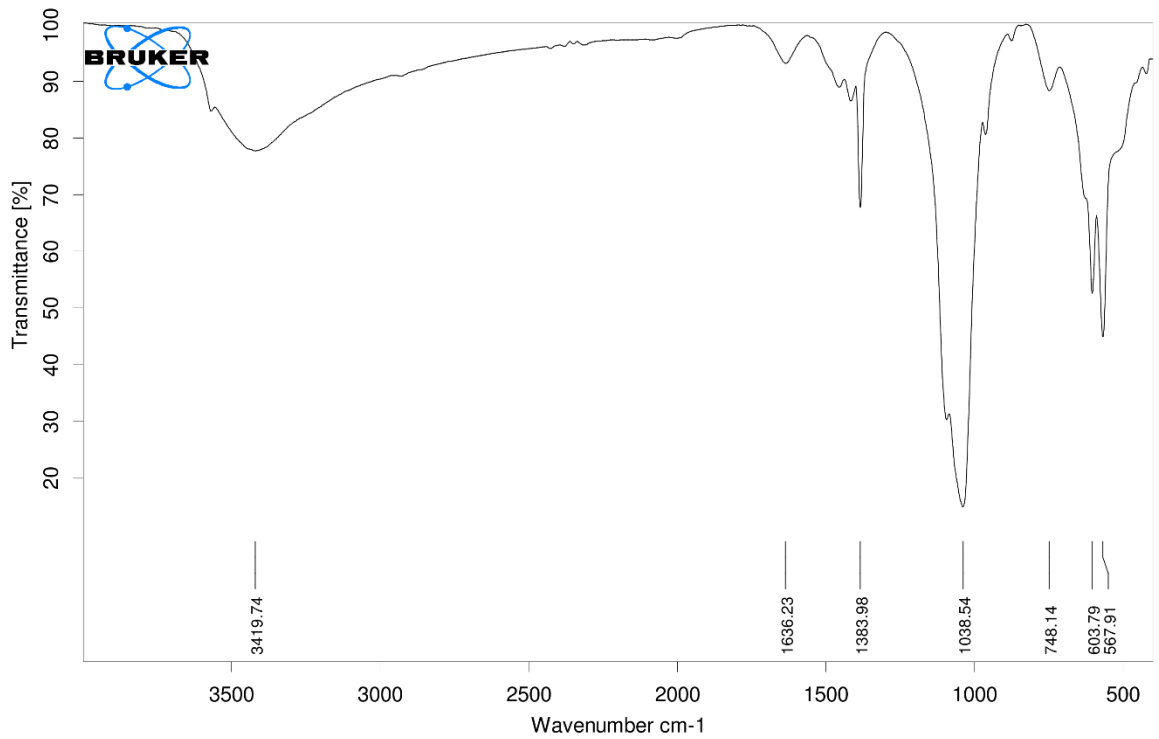

Figure 4.3: FTIR spectrum for sample of composite.

Based on the FTIR spectrum above we can analyze that-

The FTIR spectrum of the sample was analyzed to confirm the structural integrity and composition of the synthesized nano-hydroxyapatite. Key observations include:

1. O-H Stretching Vibration:

A broad band centered around 3400 cm^{-1} is attributed to the O-H stretching vibration of hydroxyl groups. This peak is primarily associated with hydroxyapatite, but contributions

from adsorbed water molecules or other hydroxyl-containing groups cannot be entirely ruled out.

2. C=C Stretching Vibration:

A weak peak observed around 1620 cm^{-1} is indicative of the C=C stretching vibration of aromatic rings. This peak is characteristic of graphene and suggests its successful incorporation into the composite. However, the intensity of this peak may be influenced by factors such as graphene loading, dispersion, and potential interactions with other components.

3. P-O Stretching Vibrations:

Two prominent peaks, centered around 1090 cm^{-1} and 960 cm^{-1}, are characteristic of the asymmetric and symmetric stretching vibrations of the P-O bond, respectively. These peaks are definitive evidence of the presence of the phosphate group in hydroxyapatite.

4. O-P-O Bending Vibration:

A peak observed around 600 cm^{-1} is assigned to the O-P-O bending vibration in the phosphate group of hydroxyapatites.

Conclusion

The FTIR analysis provides strong evidence for the successful synthesis of a graphene-ferrocene-hydroxyapatite composite. The presence of characteristic peaks corresponding to the functional groups of each component confirms their integration into the composite material. However, further investigations, such as Raman spectroscopy and X-ray diffraction, are necessary to gain deeper insights into the structural properties and interactions between the components.

4.4. X-ray Diffraction (XRD):-

X-ray Diffraction (XRD) is a powerful, non-destructive analytical technique used extensively in materials science, chemistry, geology, and engineering to study the structural properties of crystalline materials. The method provides critical insights into the atomic-scale arrangement of materials, making it an essential tool for understanding their composition, phase purity,

crystallinity, and mechanical behavior. XRD is particularly significant in fields such as pharmaceuticals, metallurgy, ceramics, and biomaterials, where the crystalline structure directly impacts the material's properties and performance.

The technique relies on the diffraction of X-rays, a phenomenon that occurs when an X-ray beam interacts with the periodic atomic planes in a crystal lattice. By measuring the angles and intensities of these diffracted X-rays, XRD can generate a characteristic diffraction pattern unique to each crystalline material. This pattern serves as a "fingerprint" that can be used to identify unknown materials, study structural defects, determine crystallite size, and even estimate residual stresses.

XRD is distinguished by its ability to analyze materials in various forms, including powders, thin films, bulk solids, and even small single crystals. Its versatility and precision make it indispensable for both academic research and industrial applications. For example, in biomaterials research, XRD is crucial for analyzing hydroxyapatite, a calcium phosphate compound widely used as a bone substitute due to its structural similarity to human bone.

One of XRD's greatest advantages is its capacity to provide direct, quantitative data about a material's internal structure without requiring extensive sample preparation. By combining this data with advanced computational tools, researchers can solve complex problems related to material performance, phase transformations, and structural stability under different conditions.

o Components of an XRD System

1. ***X-ray Source***: Produces X-rays, commonly using copper (Cu) or molybdenum (Mo) as targets to generate characteristic radiation (e.g., Cu Kα).

2. ***Specimen Holder***: Holds the sample in place, ensuring precise alignment with the X-ray beam.

3. ***Goniometer***: Controls the angular movement of the sample and detector to scan a range of diffraction angles (2θ2\theta2θ).

4. ***Detector***: Measures the intensity of diffracted X-rays at different angles. Modern detectors include scintillation counters and CCD cameras.

5. ***Monochromator***: Filters unwanted wavelengths to ensure only characteristic X-rays reach the sample.

6. ***Slits and Collimators***: Optimize the beam width and divergence for improved resolution.

7. ***Control Electronics and Software***: Coordinate the system's components, collect data, and process the diffraction patterns.

- **Working Process**

1. ***X-ray Generation***: A monochromatic X-ray beam is generated and directed at the sample.
2. ***Diffraction****:* As the X-rays interact with the crystalline planes of the material, they are scattered. Constructive interference occurs at specific angles (2θ2\theta2θ), satisfying Bragg's Law.
3. ***Detection***: Diffracted X-rays are detected, and their intensity is recorded as a function of 2θ2\theta2θ.
4. ***Data Analysis***: The resulting diffraction pattern (intensity vs. 2θ2\theta2θ) is analyzed to identify the material's crystalline phases, lattice parameters, and other structural properties.

This technique is particularly useful for characterizing materials such as hydroxyapatite, allowing for the determination of its crystallinity and phase purity.

Figure 4.4- XRD at Shivaji University Kolhapur

The X-ray Diffraction (XRD) analysis was conducted using a Bruker D2 Phaser XRD system, manufactured by Bruker Ltd., Germany. The instrument is located at Shivaji

University, Kolhapur, and is equipped with advanced capabilities for high-resolution analysis of crystalline materials.

- **XRD of composite material:**

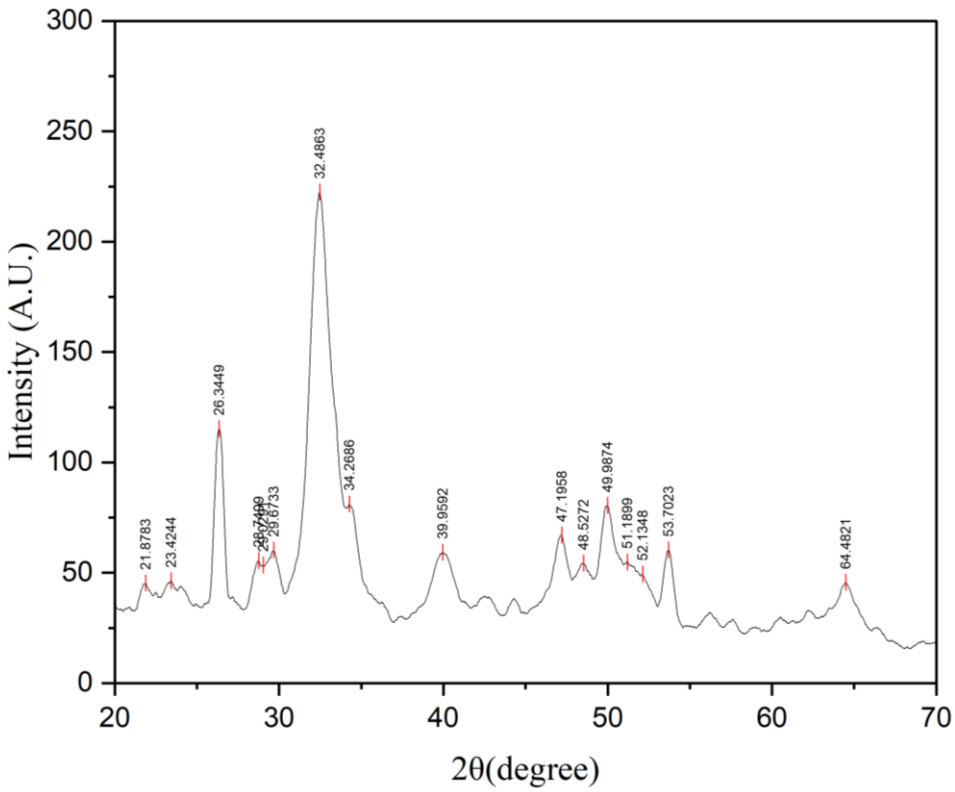

Figure 4.5:-XRD spectrum for composite.

- **XRD Analysis Observations**

1. Primary Peaks (30°–35° 2θ):

o The sharp and intense peaks in the 30°–35° region are characteristic of hydroxyapatite (HA), confirming its crystalline phase.

o These peaks align with the HA lattice reflections, particularly the (211), (112), and (300) planes.

2. Low-Angle Peak (~10° 2θ):

o This peak is not typical of pure HA and could arise due to:

- Ferrocene: Possible decomposition products or interactions involving ferrocene, potentially forming iron-containing phases.

- Calcium Carbonate or Brushite: Contaminants or secondary calcium phosphate phases.

- Organic Residues: Ferrocene or graphene precursors may leave low-angle reflections if poorly crystalline.

3. Graphene Contribution (~26° 2θ):

o Graphene typically shows a peak near 26° due to the (002) basal plane reflection. Its intensity and sharpness can vary depending on the graphene's degree of exfoliation and crystallinity.

o If no distinct peak is observed at 26°, the graphene might be in an amorphous or disordered form.

4. Potential Ferrocene Effects:

o Ferrocene itself is amorphous in bulk and may not exhibit strong peaks, but upon decomposition, it can contribute to the formation of iron-containing crystalline phases (e.g., Fe oxides or carbides). These might result in additional reflections in both low- and mid-angle regions.

5. Crystallinity and Composite Nature:

o The strong peaks in the HA region confirm high crystallinity of this phase.

o Broader or additional peaks could reflect interactions between HA, graphene, and ferrocene, suggesting the composite structure influences the overall diffraction pattern.

Conclusions:-

The XRD analysis confirms the presence of hydroxyapatite as the primary phase in the composite. Additional peaks at ~10° and ~26° suggest contributions from ferrocene decomposition products and graphene. These observations highlight the composite's multiphase nature and indicate potential interactions between HA and the added components, which could influence its overall properties.

4.5. Transmission Electron Microscopy (TEM): -

Transmission Electron Microscopy (TEM) is a powerful imaging technique used to study the structure and properties of materials at very high resolution, often down to the atomic scale. TEM works by transmitting a beam of electrons through an ultra-thin sample, allowing detailed information about the material's internal structure to be obtained.

- **Components of TEM**

1. ***Electron Gun:***
   - Generates a high-energy electron beam (usually 60-300 kV).
   - Common sources: Tungsten filament, LaB6 crystal, or field emission gun.
2. ***Condenser Lens System:***
   - Focuses and controls the electron beam's intensity and size before it hits the sample.
3. ***Specimen Holder:***
   - Holds the thin sample in a controlled environment.
   - May allow tilting, rotating, or cooling/heating for advanced studies.
4. ***Objective Lens:***
   - Main lens for focusing the electron beam through the sample.
   - Determines the primary image formation and resolution.
5. ***Intermediate and Projector Lenses:***
   - Magnify the image formed by the objective lens onto a detector.
6. ***Detectors/Imaging System:***
   - Collects the transmitted electron beam to create an image.
   - Common detectors: fluorescent screens, CCD/CMOS cameras.
7. ***Vacuum System:***
   - Maintains a high vacuum to prevent electron scattering by air molecules.
8. ***Control Electronics and Computer System:***
   - Manage alignment, focus, magnification, and image acquisition.

- **Working Principle of TEM**

The Transmission Electron Microscope (TEM) operates by generating a high-energy electron beam (60-300 kV) from an electron gun, which is focused onto an ultra-thin sample using magnetic lenses. As the beam passes through the sample, electrons interact with the material, undergoing elastic or inelastic scattering. The transmitted and scattered electrons carry information about the sample's structure and composition. Magnetic objective lenses magnify these interactions, forming a highly detailed image or diffraction pattern, which is further magnified by intermediate and projector lenses and recorded on a screen or camera.

- **Process of TEM Analysis**

1. ***Sample Preparation:***
   - Samples must be extremely thin (10–100 nm) to allow electron transmission.
   - Methods: Ultramicrotomy, focused ion beam (FIB) milling, or chemical thinning.
2. ***Loading the Sample:***
   - The specimen is mounted onto a specialized holder and inserted into the microscope.
3. ***Vacuum System Activation:***
   - The TEM chamber is evacuated to create a vacuum.
4. ***Beam Alignment:***
   - The electron beam is aligned using electromagnetic lenses and apertures.
   - Focus and intensity are adjusted.
5. ***Image Acquisition****:*
   - Electrons passing through the sample create an image with contrast arising from differences in electron scattering due to material density, thickness, or atomic number.
   - Images are magnified and recorded.
6. ***Data Analysis:***
   - The resulting images and diffraction patterns are analyzed to understand the sample's structural, morphological, and compositional details.

Figure 4.4-TEM/EDX at Shivaji University Kolhapur.

The morphology and particle size of the graphene-hydroxyapatite-ferrocene nanocomposite were characterized using Transmission Electron Microscopy (TEM). The analysis was conducted at the Common Facility Center, Shivaji University, Kolhapur, using the JEOL JEM 2100 PLUS microscope operated at an accelerating voltage of 200 kV. Samples were prepared by dispersing the composite in ethanol, followed by drop-casting onto a carbon-coated copper grid for imaging.

- **TEM of composite material: -**

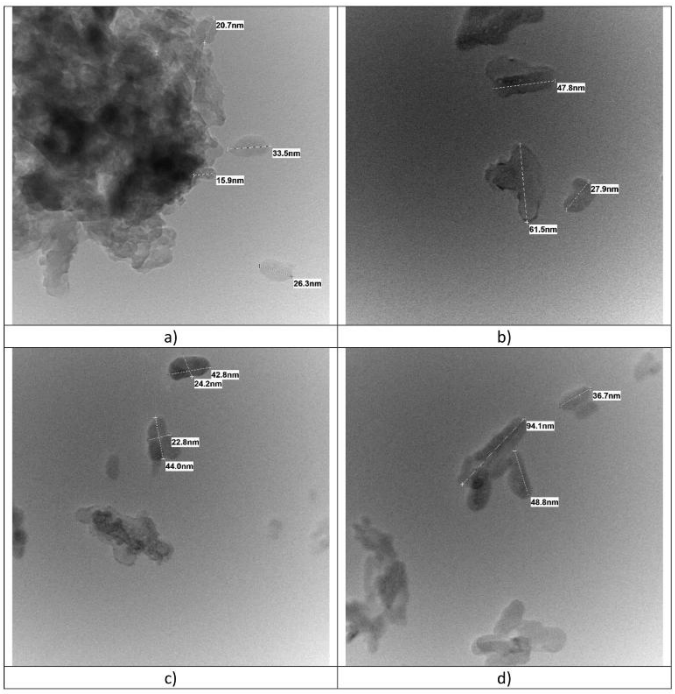

Figure 4.5: TEM images of nano composite

The TEM analysis was conducted to examine the morphology and particle size of the synthesized graphene-hydroxyapatite-ferrocene nanocomposite. The obtained images reveal nanoscale features and provide insights into the structural characteristics of the composite material.

- **Particle Size**

The observed particle dimensions range between approximately 20 nm and 60 nm, indicating the successful synthesis of the nanocomposite with nanoscale integration of the constituent materials. The size distribution suggests a uniform dispersion of the particles within the matrix, which is essential for maintaining the desired properties of the composite.

- **Morphology**

The TEM images exhibit irregularly shaped particles, with distinct variations in contrast. The layered or sheet-like structures observed in the images can be attributed to graphene, which acts as the support matrix in the composite. Smaller, denser regions likely correspond to hydroxyapatite and ferrocene particles, contributing to the functional properties of the material. These observations highlight the effective incorporation of graphene, hydroxyapatite, and ferrocene into the composite system.

- **Contrast Analysis**

The differences in contrast across the images arise from the varying electron densities of the components. The brighter regions are likely due to the presence of graphene, which has a lower electron density, while the darker regions correspond to hydroxyapatite and ferrocene, both of which are denser materials. This contrast differentiation further confirms the coexistence of the three components in the nanocomposite.

- **Conclusion**

The TEM analysis confirms the successful fabrication of the graphene-hydroxyapatite-ferrocene nanocomposite. The observed nanoscale particle sizes, irregular morphologies, and distinct contrast variations validate the integration of graphene as a matrix, hydroxyapatite as a bioactive phase, and ferrocene as a functional additive. These findings are consistent with the expected structural characteristics of the composite and provide a basis for further characterization and application studies.

4.6. Energy-Dispersive X-ray Spectroscopy (EDX)

Energy-Dispersive X-ray Spectroscopy (EDX/EDS) is an analytical technique used to determine the elemental composition of materials. It is often integrated with electron microscopy systems such as Scanning Electron Microscopy (SEM) or Transmission Electron Microscopy (TEM). EDX provides qualitative and quantitative information about the elements present in a sample.

- **Working Principle of EDX**

The EDX technique is based on the interaction of a high-energy electron beam or X-ray beam with the sample, causing the ejection of inner-shell electrons from atoms in the material. This

creates electron vacancies, which are filled by electrons from higher energy levels. When this happens, the atom emits X-rays with an energy characteristic of the specific element. These emitted X-rays are detected and analyzed by the EDX detector to identify and quantify the elements in the sample.

- **Working Process of EDX Analysis**

1. **Sample Preparation**: The sample is prepared to ensure a clean surface and, if necessary, coated with a conductive material to improve electron interaction.
2. **Electron Beam Interaction**: A focused beam of electrons (TEM) or X-rays (in standalone EDX systems) is directed onto the sample.
3. **X-ray Emission**: The high-energy beam causes the ejection of electrons from the inner shells of atoms in the sample, resulting in the emission of characteristic X-rays as higher-energy electrons fill the vacancies.
4. **X-ray Detection**: These X-rays are captured by an energy-dispersive detector, typically a silicon drift detector (SDD), which measures their energy and intensity.
5. **Data Processing**: The detector processes the X-ray signals to produce a spectrum showing the energy peaks corresponding to the elements present in the sample. The intensities of these peaks are used to estimate the concentration of the elements.
6. **Analysis and Reporting**: Software analyzes the spectrum to identify the elements and their relative abundances. The data can be displayed as a spectrum or elemental mapping over the sample's surface.

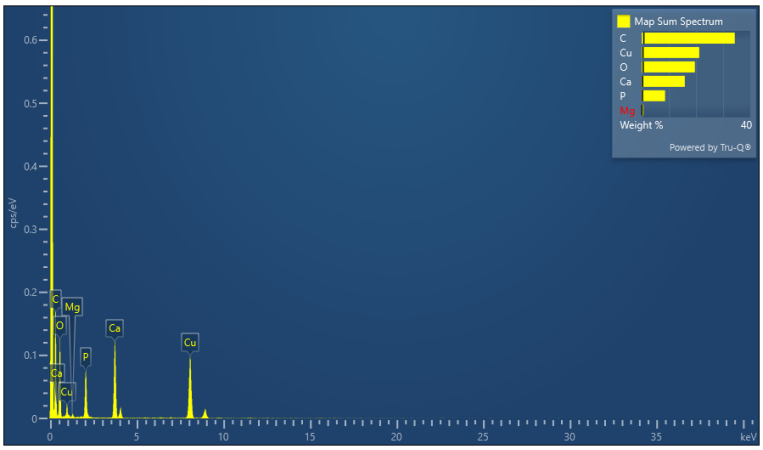

Figure 4.6- EDX of nanocomposite

Map Sum Spectrum							
Element	Line Type	k Factor	k Factor type	Absorption Correction	Wt%	Wt% Sigma	Atomic %
C	K series	2.787	Theoretical	1.00	34.29	0.73	55.91
O	K series	2.033	Theoretical	1.00	19.56	0.49	23.94
Mg	K series	1.082	Theoretical	1.00	0.57	0.09	0.46
P	K series	1.058	Theoretical	1.00	8.58	0.27	5.43
Ca	K series	0.989	Theoretical	1.00	15.83	0.33	7.73
Cu	K series	1.221	Theoretical	1.00	21.18	0.41	6.53
Total:					100.00		100.00

Table 4.1- Tabularized data of EDX.

.

- **EDX Analysis for Hydroxyapatite-Graphene-Ferrocene Composite**

- **Elemental Composition:**

The EDX spectrum provides the following elemental data for the composite:

- Carbon (C):

Wt%: 38.49%

Atomic%: 56.76%

High carbon content confirms the presence of graphene and the organic component of ferrocene.

- Oxygen (O):

Wt%: 21.50%

Atomic%: 23.80%

Indicates the presence of oxygen in hydroxyapatite and potentially graphene oxide (if partially oxidized).

- Phosphorus (P):

Wt%: 14.74%

Atomic%: 8.43%

Consistent with the phosphate group ($PO4^{3-}$) in hydroxyapatite.

- Calcium (Ca):

Wt%: 24.06%

Atomic%: 10.63%

Matches the Ca content in hydroxyapatite ($Ca_{10}(PO_4)_6(OH)_2$), supporting its inclusion in the composite.

- Iron (Fe):

Wt%: 1.21%

Atomic%: 0.38%

Confirms the presence of ferrocene, contributing to the composite structure.

- **Analysis and Interpretation:**

1. Hydroxyapatite:

- The Ca:P atomic ratio is approximately 1.26, which is close to the theoretical value of 1.67 for stoichiometric hydroxyapatite, but slightly lower. This suggests a potential deviation from perfect stoichiometry or partial substitution of calcium.

2. Graphene:

- The high carbon content (38.49 wt%) indicates a significant contribution from graphene. This aligns with the expected structure of the composite, as graphene is primarily carbon-based.

3. Ferrocene:

- The detection of iron (Fe) at 1.21 wt% confirms the presence of ferrocene in the composite. The lower atomic percentage of Fe compared to other elements aligns with the minor proportion of ferrocene in the material.

4. Oxygen Contribution:

- The oxygen content is consistent with its roles in hydroxyapatite ($PO4^{3-}$ groups) and any potential oxygen functional groups on graphene oxide.

- **Conclusion:**

The EDX analysis validates the successful synthesis of the hydroxyapatite-graphene-ferrocene composite. The elemental ratios and compositions align with the expected constituents:

- Hydroxyapatite contributes calcium, phosphorus, and oxygen.
- Graphene adds significant carbon content.
- Ferrocene introduces iron into the structure.

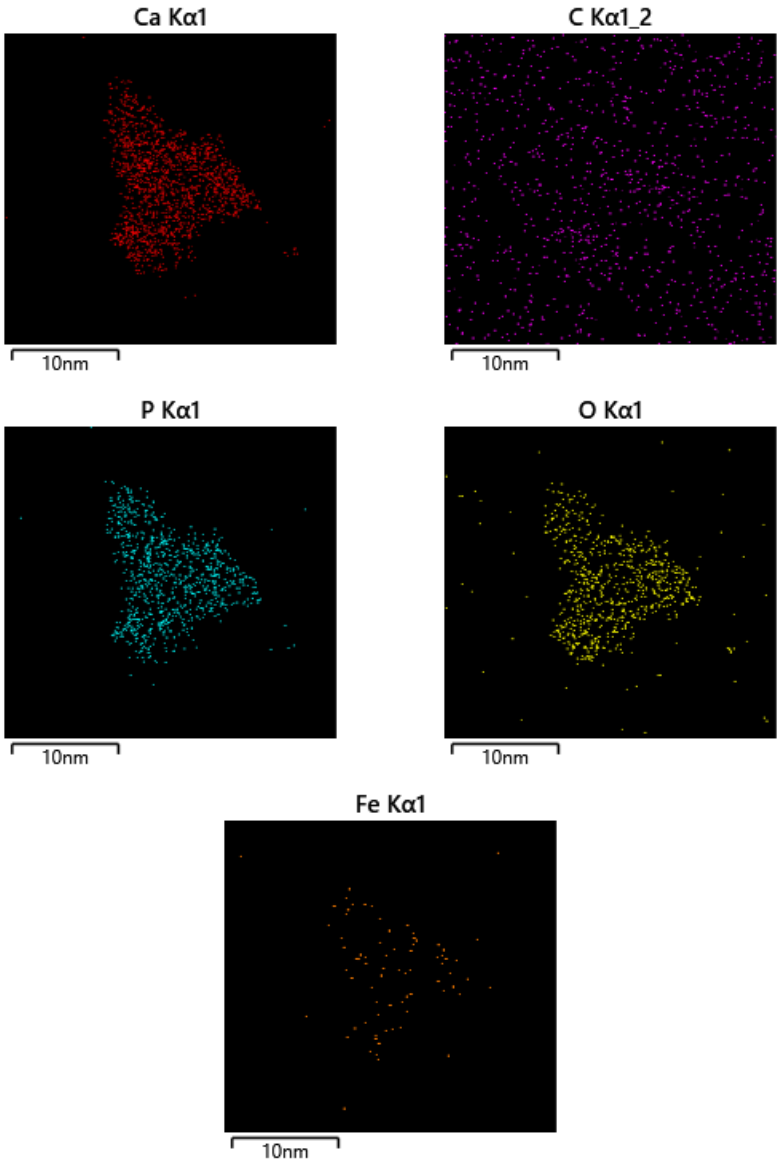

Figure 4.7-4.11- EDX mapping of elements in composite.

4.7. Raman Spectroscopy: -

Raman spectroscopy is a non-destructive analytical technique used to observe vibrational, rotational, and other low-frequency modes in a system. It is widely employed to provide molecular and structural information about a sample, identify materials, and assess chemical composition and properties.

- **Working Principle**

Raman spectroscopy is based on the Raman Effect, discovered by C.V. Raman in 1928. The principle involves inelastic scattering of monochromatic light, typically from a laser. When light interacts with a molecule, most photons scatter elastically (Rayleigh scattering), but a

small fraction scatters inelastically. This inelastic scattering results in a shift in energy corresponding to the vibrational or rotational modes of the molecules in the sample.

- **Key Concepts:**

1. ***Incident Light****:* A laser provides monochromatic light that interacts with the sample.
2. ***Elastic Scattering****:* Most photons scatter without a change in energy (Rayleigh scattering).
3. ***Inelastic Scattering****:* A small portion of photons exchange energy with molecular vibrations, causing shifts:

o *Stokes Shift*: Energy is transferred to the molecule, and the scattered photon has less energy.
o *Anti-Stokes Shift*: Energy is taken from the molecule, and the scattered photon has more energy.

These energy shifts are measured and analyzed to provide insights into molecular vibrations and structures.

- **Process of Raman Spectroscopy**

1. ***Sample Preparation:***
- The sample can be solid, liquid, or gas, and usually requires minimal preparation.

2. ***Excitation:***
- A laser beam is directed at the sample, typically in the visible, near-infrared, or near-ultraviolet range.

3. ***Scattering:***
- Photons interact with molecular vibrations, causing scattering (elastic and inelastic).

4. ***Collection of Scattered Light:***
- A spectrometer collects and filters the scattered light to isolate inelastic scattering.

5. ***Detection and Analysis:***
- The scattered light is dispersed via a grating and detected by a sensitive detector, such as a CCD (charge-coupled device).
- The resulting spectrum represents the intensity of scattered light as a function of frequency shift (Raman shift), which correlates to molecular vibrations.

Figure 4.12- Raman Spectrometer at Shivaji University Kolhapur

Raman spectroscopy has diverse applications across scientific and industrial fields. It is widely used for material identification, enabling the detection of organic and inorganic compounds through their unique vibrational fingerprints. In structural analysis, it provides insights into crystal structures, phase transitions, and mechanical stresses in materials. The technique is instrumental in chemical composition studies, offering non-destructive analysis of mixtures to determine substance concentrations. It plays a crucial role in nanotechnology, characterizing materials such as graphene and carbon nanotubes, and in environmental science, it assists in pollutant detection.

The Raman spectroscopy analysis was performed using a Bruker Ltd., Germany, Model: MultiRAM spectrometer available at Shivaji University, Kolhapur. The MultiRAM is a high-performance FT-Raman spectrometer equipped with a Nd:YAG laser operating at a wavelength of 1064 nm, offering a spectral range of 3600–36 cm^{-1} and a resolution of 0.5 cm^{-1}. It features a liquid nitrogen-cooled Ge detector for enhanced sensitivity and supports both 180° and 90° measurement geometries, making it versatile for advanced material characterization. This setup is particularly effective for reducing fluorescence interference, allowing precise analysis of diverse samples such as composites, biomaterials, and nanostructures.

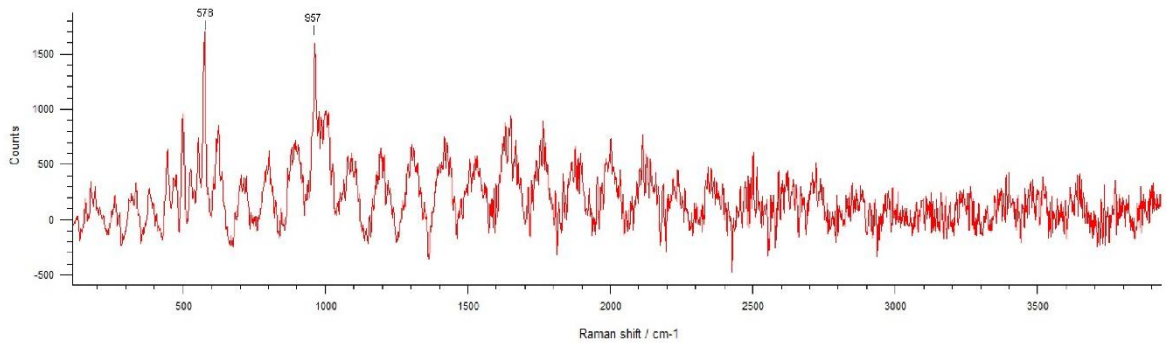

Figure 4.13- Raman spectroscopy graph of nano composite

- **Raman Spectroscopy Analysis**

The Raman spectrum shows the following significant peaks and their corresponding assignments:

Observed Peaks:

1. 461 cm^{-1}:

Associated with the bending vibrations of phosphate groups ($PO4^{3-}$) in hydroxyapatite (HA).
Indicates the presence of HA's crystalline structure.

2. 547 cm^{-1} and 608 cm^{-1}:

Symmetric and asymmetric stretching vibrations of phosphate groups in HA.
These peaks confirm the integrity of the HA phase in the composite.

3. 797 cm^{-1}:

This peak could be attributed to additional structural vibrations, potentially indicating an interaction between graphene and hydroxyapatite.

4. 1408 cm^{-1}:

Corresponds to the D-band of graphene, which is associated with structural defects, edges, or functional groups in graphene sheets.

5. 2000-3000 cm^{-1} range (broad features):

This range could potentially include the G-band (around 1580 cm^{-1}) and 2D-band (around 2700 cm^{-1}) of graphene.

The G-band represents the in-plane vibrations of sp^2 carbon atoms, while the 2D-band is indicative of the layer structure of graphene.

- **Interpretation:**

Hydroxyapatite: The phosphate vibrational peaks (461 cm^{-1}, 547 cm^{-1}, 608 cm^{-1}) confirm the presence of HA in the composite. These peaks are well-defined, indicating a crystalline HA phase.

Graphene: The D-band (1408 cm^{-1}) and possible G/2D-band features indicate the successful incorporation of graphene into the composite. The D-band suggests some level of defects or functionalization in the graphene, which may enhance its interaction with HA.

Composite Interaction: The combination of HA and graphene is evidenced by peak shifts or new vibrations, such as the feature at 797 cm^{-1}. This suggests possible chemical or physical interactions between the two components.

Conclusion:

The Raman spectrum confirms the presence of both hydroxyapatite and graphene in the composite. The distinct peaks validate their structural integrity while also suggesting interactions that contribute to the composite's unique properties.

4.8. Thermogravimetric Analysis/Differential Thermal Analysis (TGA/DTA):

Thermal analysis techniques are essential for understanding the thermal properties and stability of materials, and among these methods, Thermogravimetric Analysis (TGA) and Differential Thermal Analysis (DTA) are widely used. These methods provide critical insights into the behaviour of materials under controlled temperature conditions, making them invaluable in fields such as material science, polymer technology, pharmaceuticals, and ceramics.

Thermogravimetric Analysis (TGA) is a technique used to measure the mass change of a material as a function of temperature or time in a controlled environment. This method is particularly useful for studying processes like decomposition, oxidation, reduction, and the

release of volatile compounds, such as moisture or gases. By monitoring these changes, TGA allows for the determination of thermal stability, the identification of material components, and the evaluation of residual contents. For instance, in polymers, TGA is often employed to measure the thermal decomposition temperature, providing data critical for understanding a material's operational limits.

Differential Thermal Analysis (DTA) complements TGA by providing information about the thermal events occurring within a material, such as melting, crystallization, and phase transitions. In DTA, the temperature difference between the sample and an inert reference material is recorded as both are subjected to the same heating program. This results in a DTA curve where endothermic and exothermic peaks reveal key thermal properties, such as melting points, heat of fusion, or phase transitions. By combining DTA with TGA, one can correlate mass loss events with specific thermal reactions, offering a more comprehensive analysis of the material.

- **Working Principle**

DTA measures the temperature difference between a sample and an inert reference material as they are subjected to the same temperature program. This technique identifies endothermic (heat-absorbing) and exothermic (heat-releasing) processes such as melting, crystallization, or phase transitions.

- **Process**

1. ***Sample and Reference Setup***: The sample and an inert reference material (e.g., alumina) are placed in separate crucibles.
2. ***Heating****:* Both are heated simultaneously under the same conditions.
3. ***Temperature Monitoring***: A thermocouple measures the temperature difference between the sample and the reference.
4. ***Data Analysis****:* A DTA curve is generated, with peaks representing endothermic and exothermic events.

TGA/DTA gives the following information about any sample

Material Decomposition: TGA is widely used to determine the thermal stability, degradation temperatures, and moisture or volatile content in polymers, composites, or ceramics.

Phase Transition Studies: DTA helps study melting points, crystallization, and other thermal events.

Purity Analysis: Identifies impurities in materials by analyzing thermal events.

Compatibility Testing: Used in drug formulation to study interactions between ingredients.

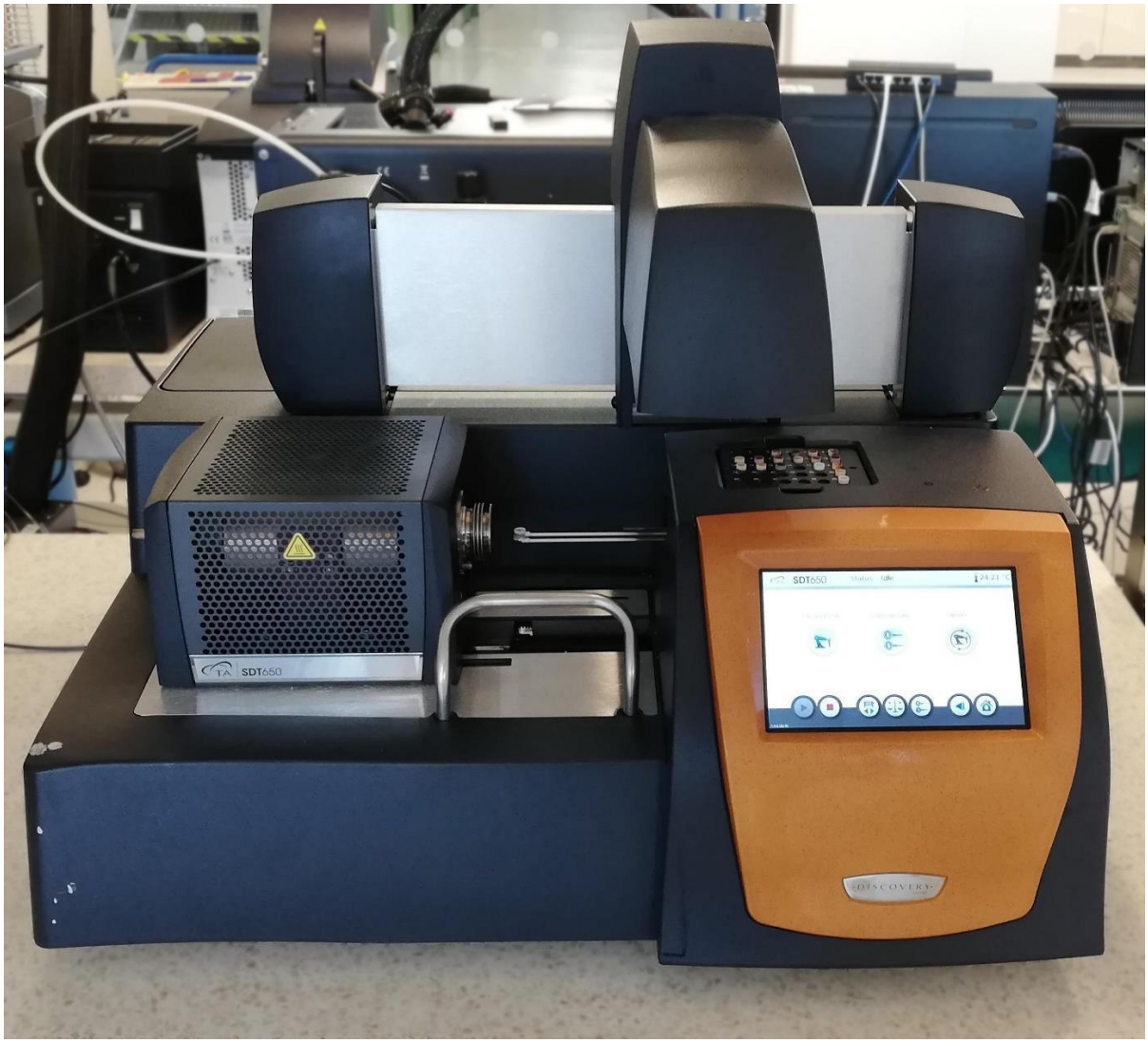

Figure 4.14 - TGA/DTA at Shivaji University Kolhapur

The thermal analysis was carried out using a TGA/DTA instrument (Make: TA Instruments, Model: SDT 650) available at Shivaji University, Kolhapur. The SDT 650 is a simultaneous TGA and DTA/DSC system capable of operating at temperatures up to 1500°C with a dynamic temperature precision of ±0.5°C. It offers a heating rate range of 0.1 to 100°C/min and a sample weight capacity of up to 200 mg, making it ideal for precise thermal and compositional analysis under controlled conditions.

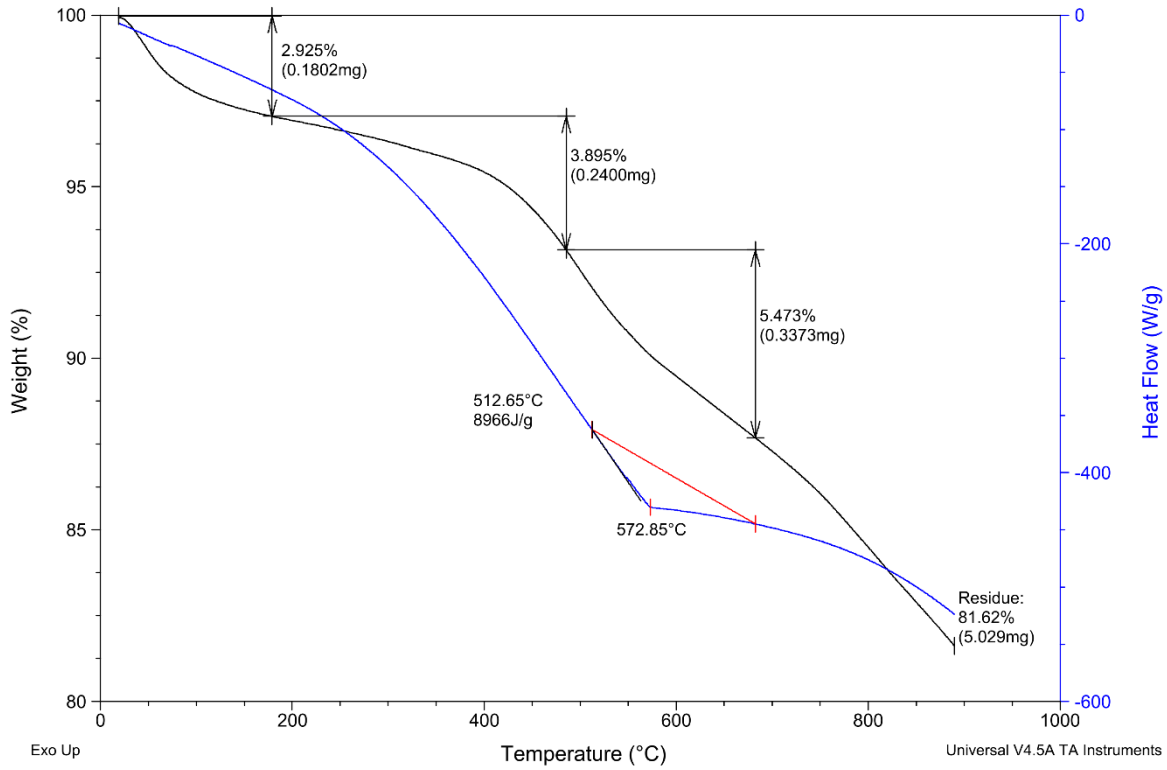

Figure 4.15 - TGA graph of nano composite.

- **Thermogravimetric Analysis (TGA) of nanocomposite:-**

Thermogravimetric analysis (TGA) of the nano composite was carried out over a temperature range of 0°C to 1000°C in an air atmosphere at a heating rate of 10°C/min. The analysis revealed excellent thermal stability, as evidenced by the retention of 95.48% of the initial mass at the end of the heating process.

Observed Thermal Events:

1. Initial Thermal Behaviour:

The sample exhibited negligible weight loss up to approximately 465°C, indicating the absence of low-temperature volatile components or significant thermal decomposition.

2. Minor Weight Loss Events:

A 1.376% weight loss (0.06272 mg) occurred near 465.84°C, likely attributed to the evaporation of adsorbed moisture or other light volatiles.

A subsequent 1.580% weight loss (0.07203 mg) was observed near 495.85°C, possibly due to the decomposition of small amounts of organic or less stable components within the composite.

3. Residual Mass:

At the conclusion of the analysis, 95.48% of the original sample mass (4.354 mg) remained, signifying a predominantly thermally stable composition, likely dominated by inorganic or high-temperature-resistant materials.

- **Interpretation:**

The minor weight losses observed near 465.84°C and 495.85°C suggest that the material undergoes minimal thermal degradation, with no major decomposition or structural breakdown evident throughout the tested temperature range. The high residual mass indicates that the nano composite is composed largely of stable components capable of withstanding prolonged exposure to elevated temperatures.

Conclusion:

The TGA results confirm the nano composite's suitability for high-temperature applications, as it demonstrates exceptional thermal stability, minimal decomposition, and high residue retention even at 1000°C. These properties suggest potential utility in environments requiring robust thermal performance.

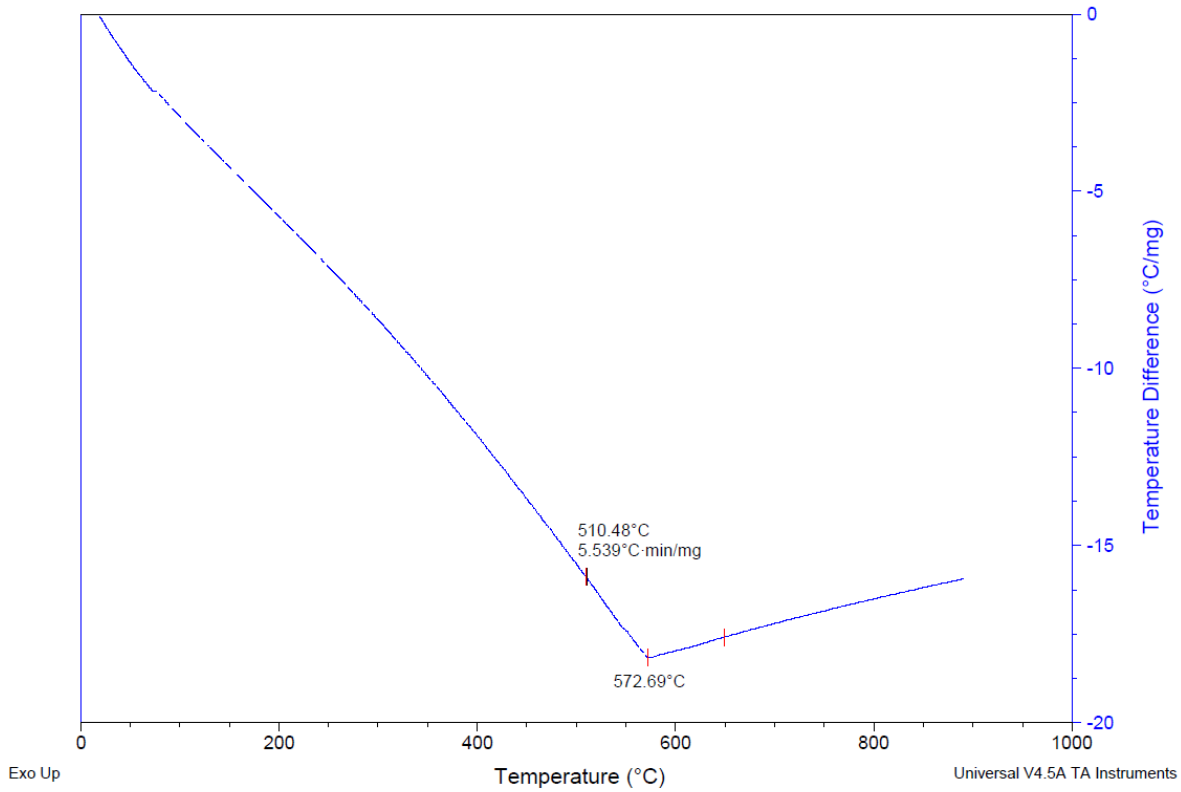

Figure 4.16- DTA graph of Nano composite

- **DTA analysis of nanocomposite sample: -**

The Differential Thermal Analysis (DTA) of the nano composite was conducted over a temperature range of 0°C to 1000°C in an air atmosphere at a heating rate of 10°C/min. The DTA graph captures the temperature difference (°C/mg) between the sample and a reference material, indicating heat absorption (endothermic) or release (exothermic).

Key Observations from the DTA Graph:

1. Endothermic Dip at ~150°C:

A clear endothermic dip is observed at approximately 150°C. This likely corresponds to the evaporation of adsorbed moisture or the release of physically bound volatile components within the composite.

The dip is relatively minor, suggesting a small energy input is required for this process, and it does not significantly impact the material's structural integrity.

2. Beyond 150°C (150–1000°C):

Following the dip at 150°C, the DTA curve remains stable without significant endothermic or exothermic events.

This indicates that the material does not undergo further thermal reactions, such as phase transitions, decomposition, or chemical changes, up to 1000°C.

- **Interpretation:**

The endothermic activity around 150°C suggests the loss of adsorbed moisture or minor volatiles. The absence of additional thermal events across the rest of the temperature range confirms the nano composite's high thermal stability and resistance to degradation or phase transformations.

- **Conclusion:**

The DTA results reveal a single thermal event at approximately 150°C, likely due to the release of moisture or volatiles. Beyond this point, the material demonstrates exceptional thermal stability, making it well-suited for applications requiring robust performance at elevated temperatures.

- **Conclusion of TGA/DTA:-**

The TGA and DTA analyses of the nano composite reveal excellent thermal stability. The TGA results show that 95.48% of the material's mass remains intact up to 1000°C, with

minor weight losses at approximately 465.84°C and 495.85°C, likely due to the release of volatiles. The DTA analysis highlights a single endothermic dip at around 150°C, suggesting the evaporation of adsorbed moisture or light volatiles. Beyond this, no significant thermal events were observed, confirming the material's stability. These results indicate that the nano composite is well-suited for high-temperature applications due to its minimal thermal degradation and robust performance.

4.8 BET Surface Area Analysis:

BET Surface Area Analysis is a technique used to measure the specific surface area of materials. It is named after the scientists Brunauer, Emmett, and Teller, who developed the BET theory. The method is widely used in materials science, including characterizing catalysts, adsorbents, and powders. It provides critical insights into the textural properties of a material by quantifying the accessible surface area available for adsorption. This information is essential for understanding and optimizing the performance of materials in various applications, such as catalysts, adsorbents, battery materials, pharmaceuticals, and porous materials like zeolites and activated carbons.

The specific surface area refers to the total surface area per unit mass of a material. It directly influences a material's reactivity, adsorption capacity, and interaction with other substances.

The BET method is based on the physical adsorption of gas molecules onto a solid surface. It assumes:

1. ***Monolayer Adsorption***: A layer of adsorbate gas molecules forms on the solid surface.
2. ***Multilayer Adsorption***: Above the monolayer, additional layers of gas molecules can adsorb.
3. ***Equilibrium Pressure****:* Adsorption occurs until an equilibrium is established between the adsorbed molecules and the gas phase.

By measuring the volume of adsorbed gas at various relative pressures, the BET equation is used to determine the specific surface area.

Process

1. ***Sample Preparation:***

o The sample is degassed to remove moisture and contaminants that might interfere with gas adsorption.

2. ***Gas Adsorption:***

o A gas (commonly nitrogen) is introduced into the chamber containing the sample.

o The pressure of the gas is gradually increased to allow adsorption.

3. ***Measurement:***

o The volume of gas adsorbed at different pressures is recorded.

o This data is used to generate an adsorption isotherm, plotting adsorbed gas volume against relative pressure.

Key Considerations

- ***Degassing****:* Proper degassing is critical for accurate results.
- ***Adsorbate Selection***: The choice of adsorbate gas depends on the material and temperature (e.g., nitrogen at 77 K for most samples).
- ***Surface Heterogeneity***: BET assumes uniform adsorption energy; deviations may occur in heterogeneous surfaces.

This technique is critical for applications in catalysis, pharmaceuticals, and nanomaterials, where surface area influences material properties.

The surface area and porosity analysis were conducted using a BET surface analyzer available at Shivaji University, Kolhapur. The instrument operates within a temperature range of 20–300°C, with a surface area measurement range from 0.1 m^2/g to no known upper limit, and a pore size range of 0.35–400 nm. It provides highly accurate measurements with an accuracy of ±0.1% of the span, making it suitable for detailed characterization of surface properties and pore structures.

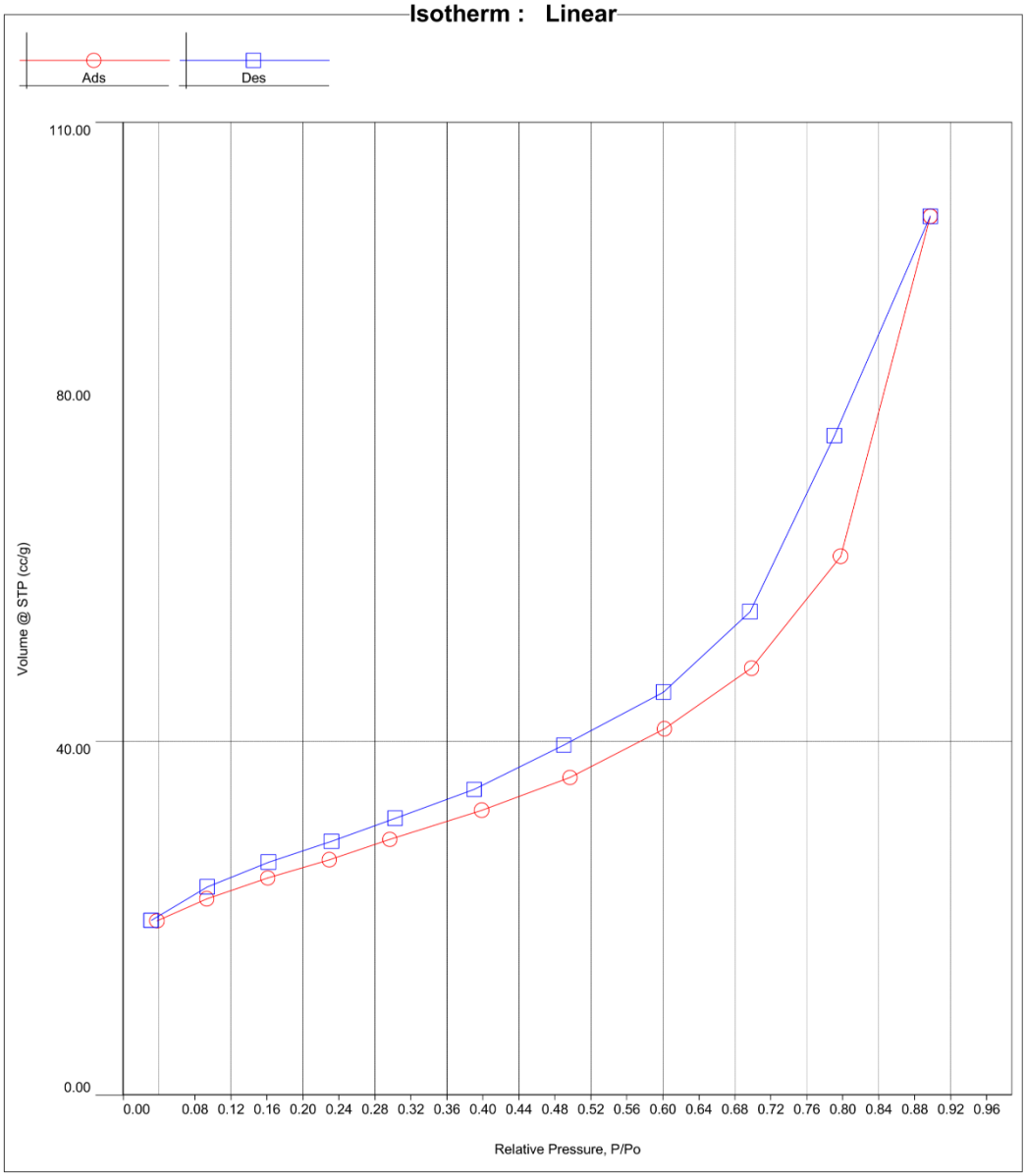

Figure 4.17- Absolute Pressure vs Volume

Analysis
Operator: Satyajeet **Date:**2025/02/11
Sample ID: - **Filename:**

Report
Operator: Satyajeet **Date:**2025/02/10
ABS2 RIT.qps

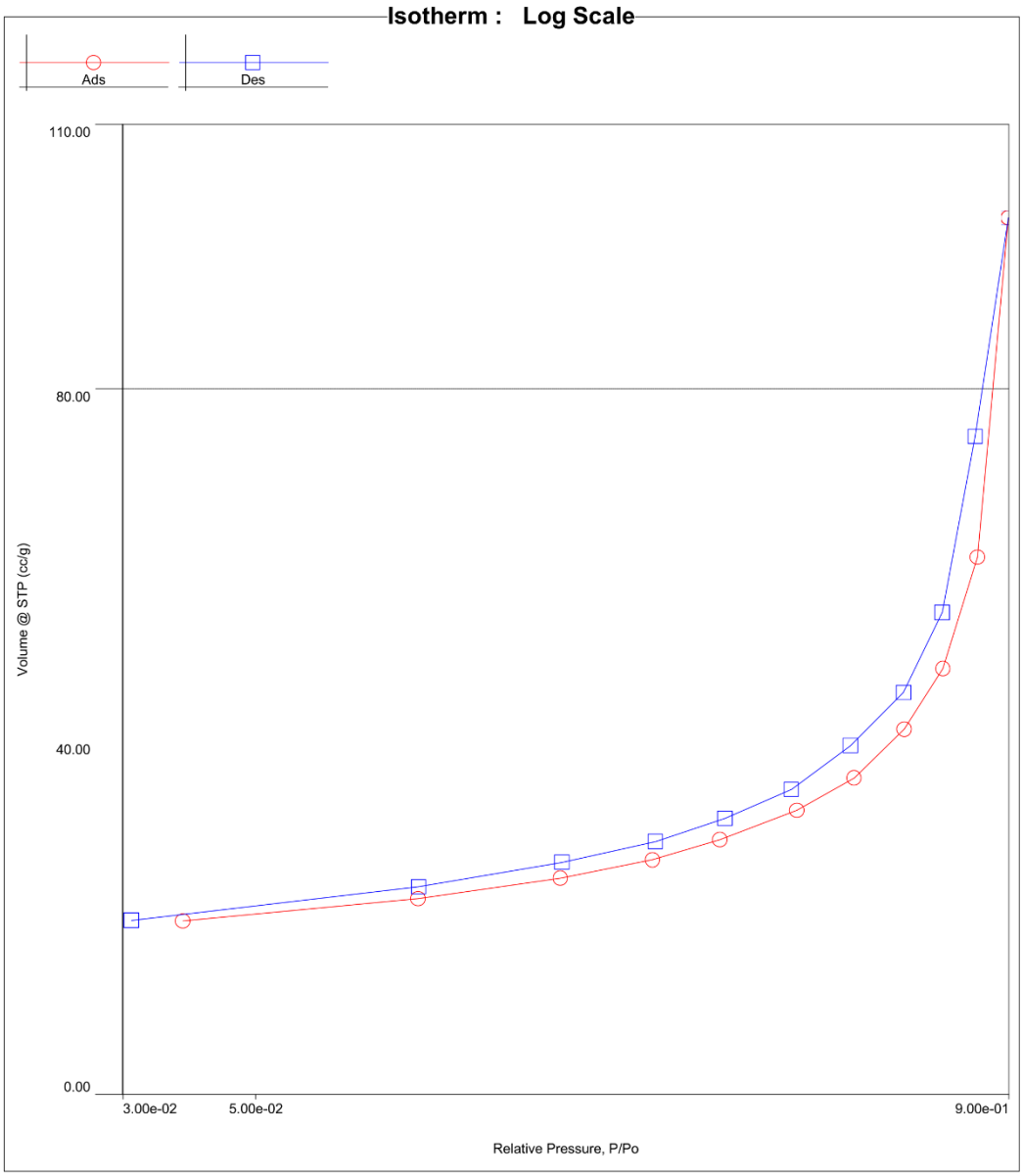

Figure 4.18-Data on Log scale

Analysis
Operator: Satyajeet **Date:**2025/02/11
Sample ID: - **Filename:**

Report
Operator: Satyajeet **Date:**2025/02/10
ABS2 RIT.qps

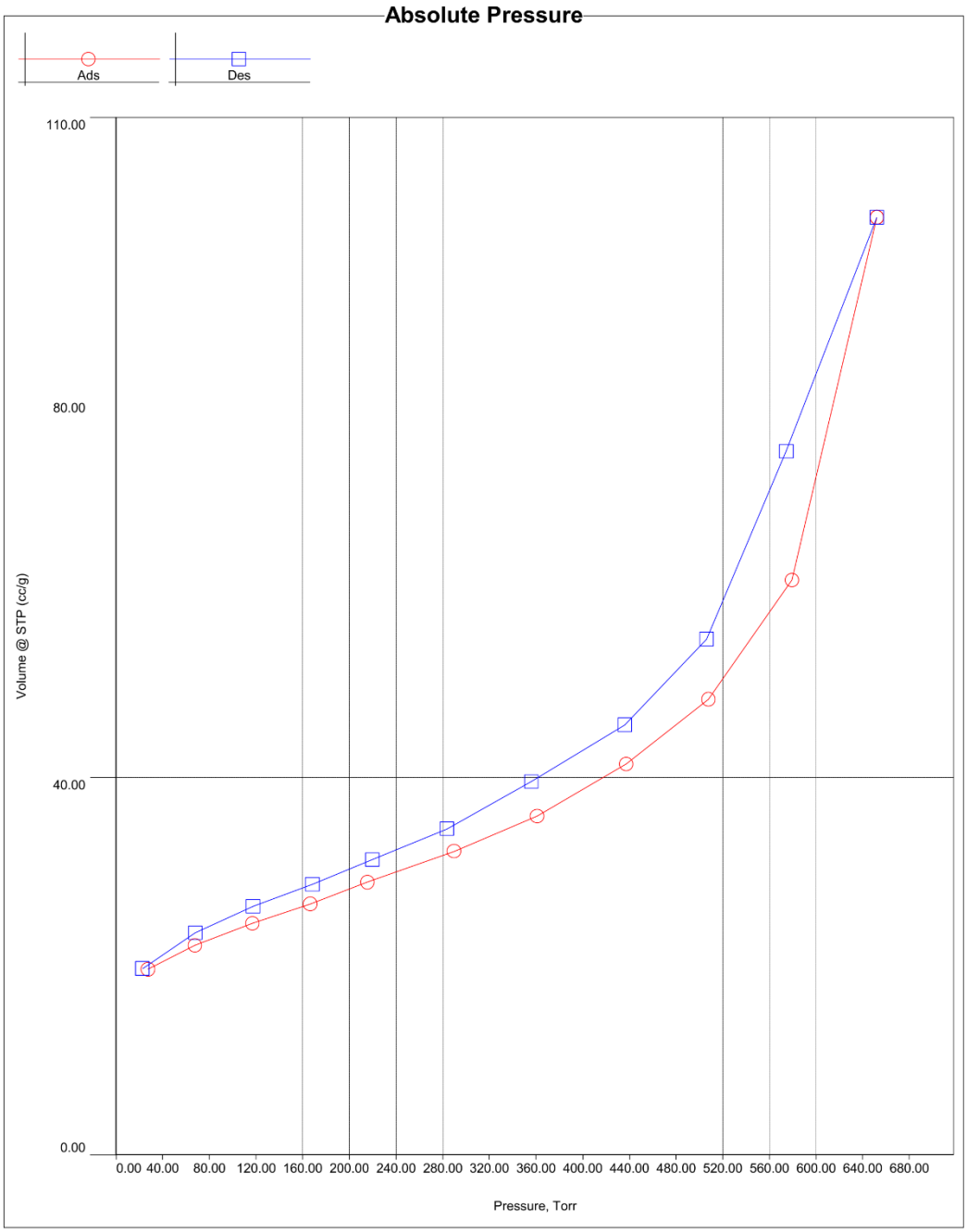

Figure 4.19- Absolute Pressure vs Volume

Analysis
Operator: Satyajeet **Date:**2025/02/11
Sample ID: - **Filename:**

Report
Operator: Satyajeet **Date:**2025/02/10
ABS2 RIT.qps

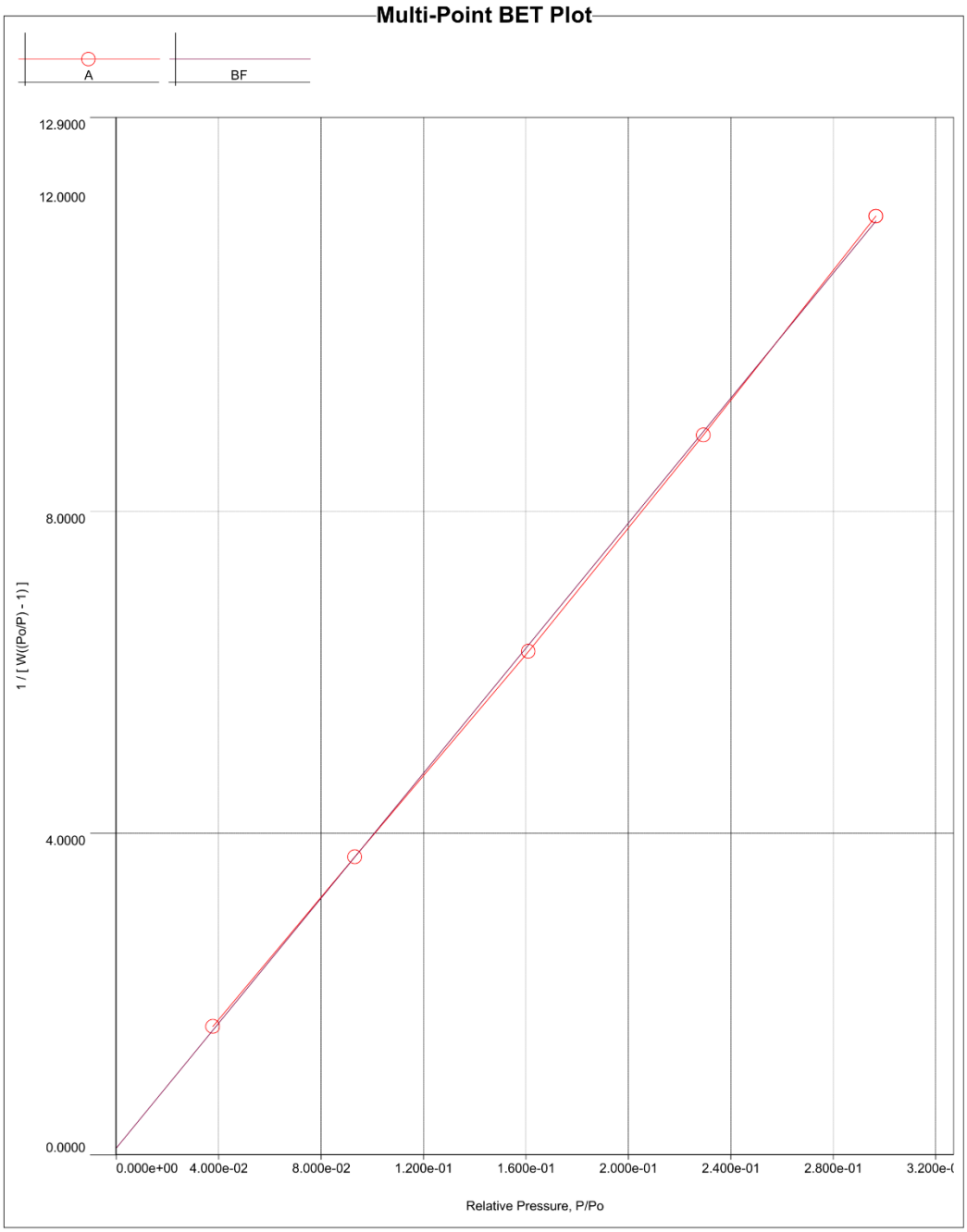

Figure 4.20- Multi point BET plot

Analysis
Operator: Satyajeet **Date:**2025/02/11
Sample ID: - **Filename:**

Report
Operator: Satyajeet **Date:**2025/02/10
ABS2 RIT.qps

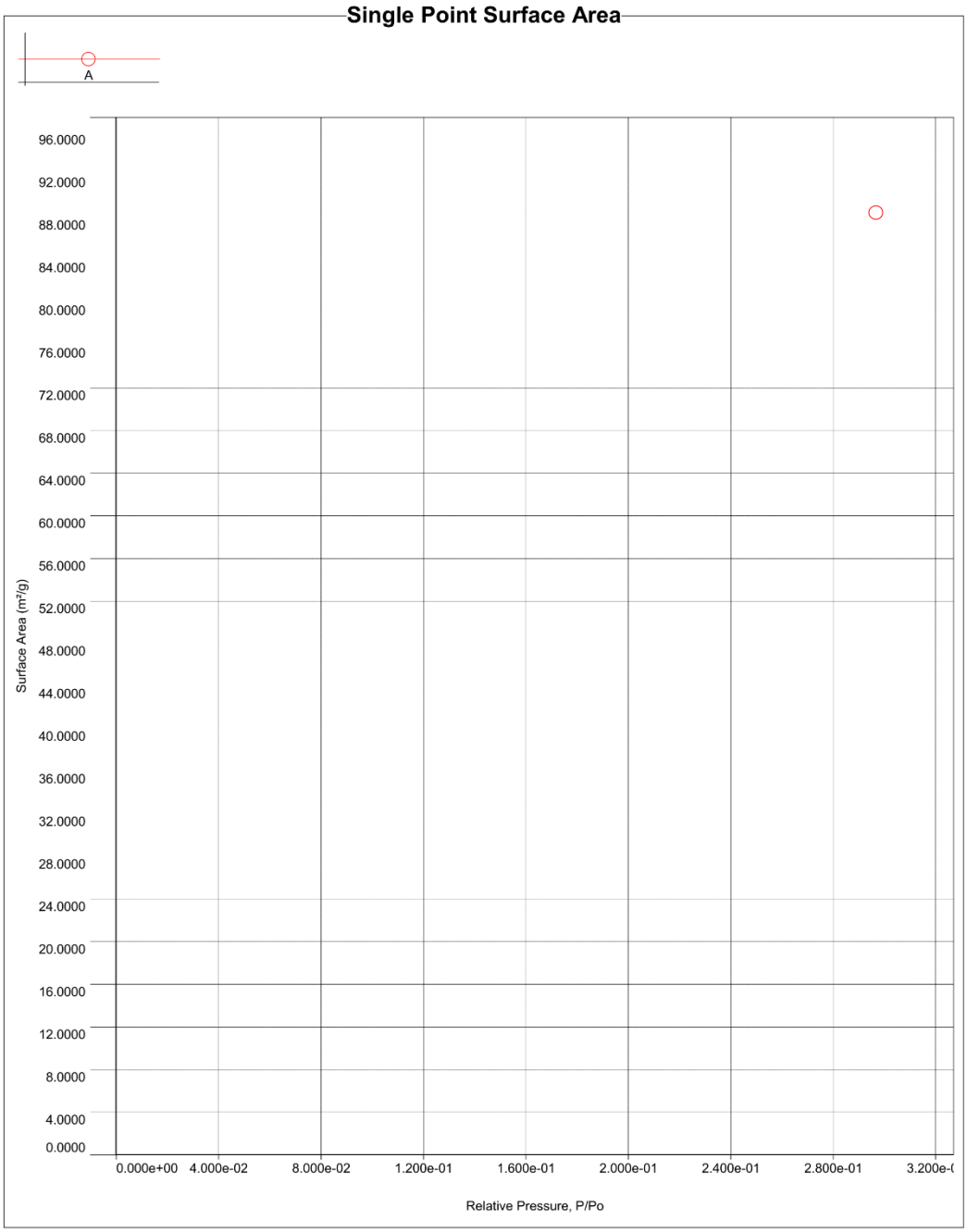

Figure 4.21- Single point surface area

Analysis
Operator: Satyajeet **Date:**2025/02/11
Sample ID: - **Filename:**

Report
Operator: Satyajeet **Date:**2025/02/10
ABS2 RIT.qps

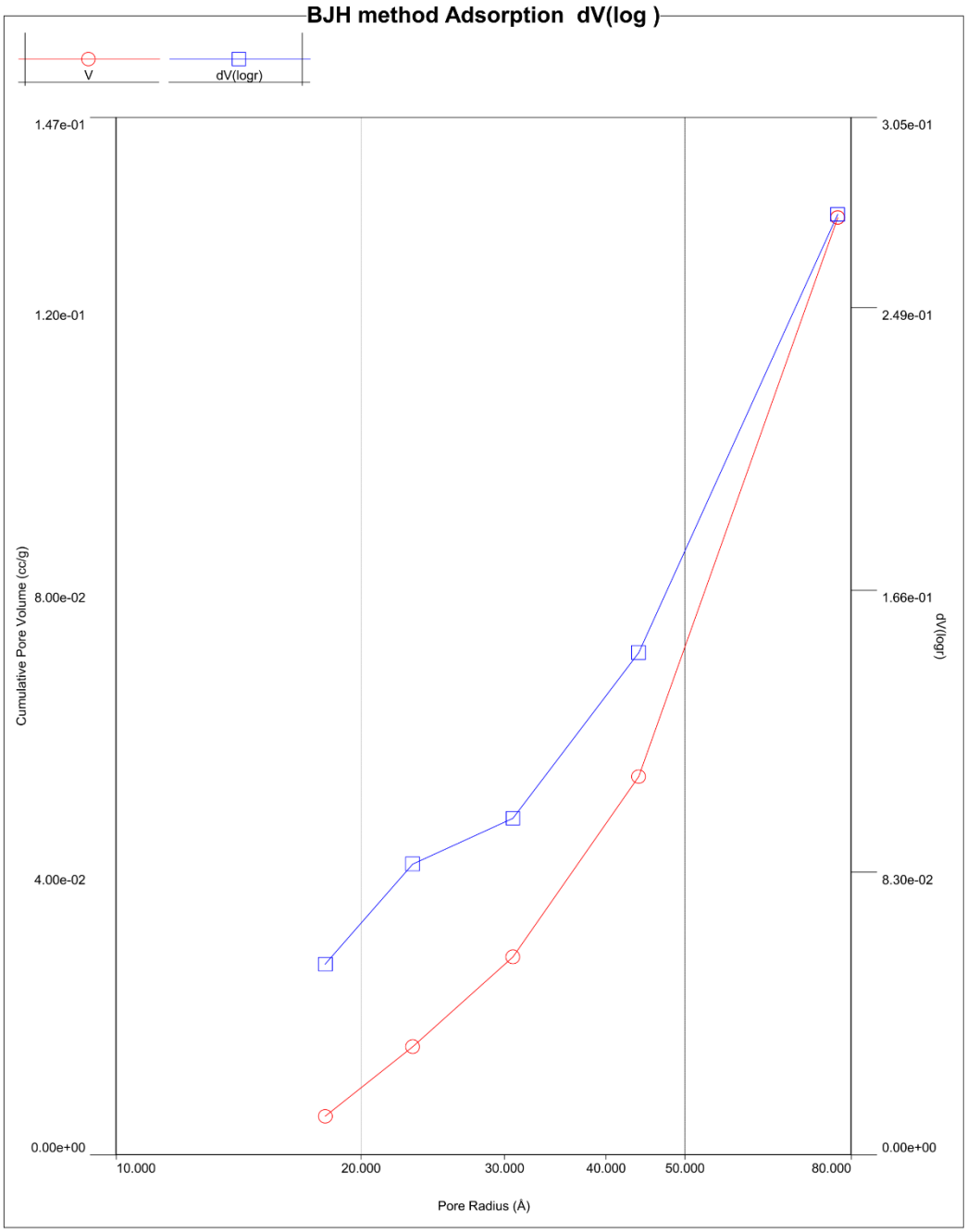

Figure 4.22- Pore size distribution (adsorption).

Analysis
Operator: Satyajeet **Date:**2025/02/11
Sample ID: - **Filename:**

Report
Operator: Satyajeet **Date:**2025/02/10
ABS2 RIT.qps

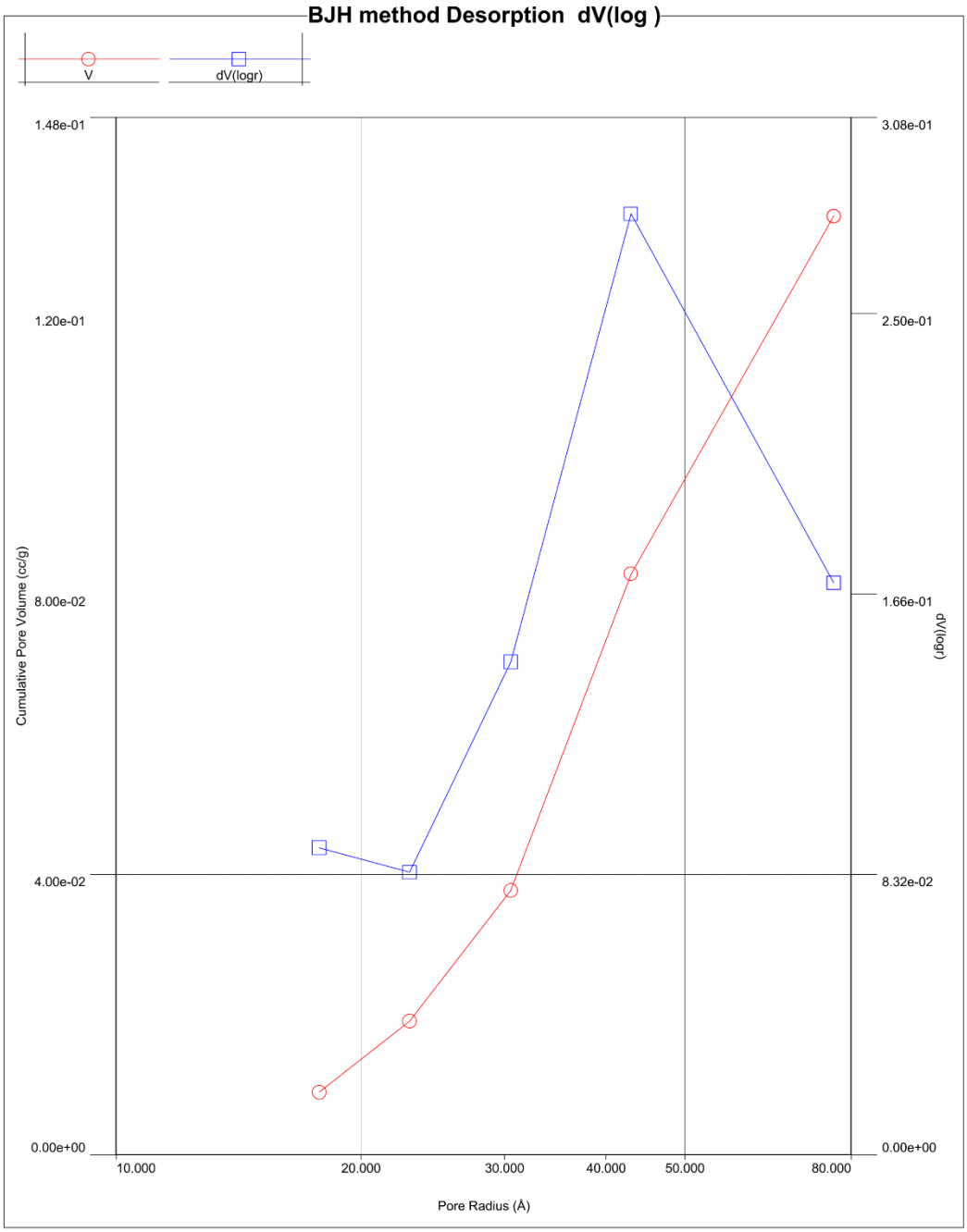

Figure 4.23- Pore size distribution (desorption)

The graphs shows nanocomposite sample using nitrogen adsorption at 273 K. The study focuses on understanding the sample's surface area, pore volume, and pore size distribution, which are critical for applications in catalysis, adsorption, and material science.

Instrument & Method:

- The analysis was conducted using a Quanta chrome Nova Win system.
- Nitrogen was used as the adsorbate gas at a bath temperature of 273 K.
- Outgassing was performed for 3 hours at 300°C to remove adsorbed impurities.

Sample Details:

- Sample Weight: **0.12 g**
- Sample Volume: **0.03077 cc**

Analysis Parameters:

- Pressure Tolerance: 0.100 Torr (adsorption/desorption)
- Equilibration Time: 60 seconds
- Outgassing Temperature: 300°C

- **Analyzing graphs:**

1. Isotherm: Linear Scale (Volume @ STP vs. Relative Pressure P/P0)

- Description: This graph plots the volume of nitrogen adsorbed per gram of the sample (at standard temperature and pressure) against relative pressure (P/P0).
- Key Observations:

o The initial steep slope at P/P0 indicates micropore filling, characteristic of high-energy adsorption sites.

o A gradual rise in the curve at higher P/P0 suggests multilayer adsorption on mesopores and macropores.

o No distinct plateau was observed, indicating that the surface is not completely saturated, which is typical of mesoporous materials.

2. Isotherm: Log Scale

- Description: This graph presents the same isotherm data on a logarithmic scale for better visualization of the low-pressure region.
- Key Observations:

o The low-pressure region shows a sharp rise in adsorbed volume, confirming significant microporous behavior.

o The logarithmic scale highlights the transition from micropore to mesopore adsorption.
o Useful for analyzing micropore filling, which dominates in the early stages of adsorption.

3. Absolute Pressure vs. Volume

- Description: This graph plots the volume of nitrogen adsorbed versus the absolute pressure (in Torr).
- Key Observations:

o The adsorption process increases steadily with rising pressure, confirming the presence of mesopores and macropores.
o This graph is primarily used to confirm the isothermal behavior of the system.

4. Multi-Point BET Plot

- Description: A linear plot used to calculate the BET surface area from the slope and intercept of the 1/[W(P/P0-1)] vs. (P/P0).
- Key Observations:

o The linear region in the plot (typically P/P0 between 0.05 and 0.3) indicates the valid range for applying the BET theory.
o High correlation (r=0.999871) confirms the reliability of the BET surface area calculation (105.6 m^2/g).

5. Single Point Surface Area

- Description: A graph showing the surface area calculated at a single point (P/P0) as a function of relative pressure.
- Key Observations:

o The graph validates the single-point BET surface area calculation (104.6 m^2/g), which is close to the multi-point value.
o Highlights that adsorption primarily occurs in the mesopores.

6. BJH Pore Size Distribution (Adsorption)

- Description: This graph uses the BJH (Barrett-Joyner-Halenda) method to plot the derivative pore volume (dV/d log(r))
- versus pore size.
- Key Observations:

o The peak around 76.50 Å indicates the predominant pore size.
o The distribution confirms the material's mesoporous nature.

o Broader peaks indicate the presence of a range of pore sizes, which could affect material performance in specific applications.

7. BJH Pore Size Distribution (Desorption)

- Description: Similar to the adsorption BJH graph, this plots the derivative pore volume (dV/d log(r))
- during desorption.
- Key Observations:

o The peak at 44.60 Å shows a smaller effective pore size during desorption, attributed to capillary condensation and hysteresis.
o The hysteresis loop observed in the desorption branch is typical of mesoporous materials.

Insights from the Graphs

1. ***High Surface Area***: The BET analysis from both single-point and multi-point methods consistently shows a large surface area (~105 m^2/g), confirming the sample's mesoporous structure.

2. ***Mesoporosity****:* The BJH pore size distribution and isotherm analysis indicate a predominance of mesopores (~40–76 Å).

3. ***Hysteresis****:* The difference between adsorption and desorption curves in the BJH method suggests pore connectivity and capillary effects.

Results and Discussion

Surface Area

- BET Surface Area (Multi-point): 105.6 m^2/g
- Single Point BET Surface Area: 104.6 m^2/g
- Langmuir Surface Area: 84.36 m^2/g

The multi-point BET surface area measurement is reliable and consistent with the single-point BET result, suggesting that the sample has a significant external and internal surface area. The Langmuir surface area is slightly lower due to its assumption of a monolayer adsorption model, which does not fully account for multilayer adsorption in porous materials.

Pore Volume

- Total Pore Volume (pores < 100 Å): 0.2205 cc/g
- BJH Adsorption Pore Volume: 0.2045 cc/g
- BJH Desorption Pore Volume: 0.2152 cc/g

The total pore volume indicates a moderate porosity, which complements the large surface area, confirming the mesoporous nature of the sample.

Pore Radius

- Average Pore Radius (BET): 41.75 Å (4.175 nm)
- BJH Adsorption Mode Pore Radius: 76.50 Å (7.65 nm)
- BJH Desorption Mode Pore Radius: 44.60 Å (4.46 nm)

The average pore size categorizes the sample as mesoporous (pore sizes between 2–50 nm), as per IUPAC classification. The BJH adsorption results show larger pore sizes than desorption, which is attributed to the hysteresis effect commonly observed in mesoporous materials.

Pore Size Distribution

The BJH method provided a detailed distribution:

- **Adsorption Curve**: Pores are predominantly within the mesoporous range, centered around 76.50 Å.
- **Desorption Curve**: Slightly smaller pores dominate, centered around 44.60 Å. This difference arises due to capillary condensation and hysteresis.

- **Interpretation of Results**

1. High Surface Area:

- The large specific surface area (~105 m^2/g) suggests enhanced interaction with biological tissues, which can improve osseointegration—a critical factor for bone pin applications.

2. Mesoporosity:

- The average pore size (~41.75 Å) falls within the mesoporous range, enabling potential for drug loading and controlled release, which can aid in reducing post-surgical infections and enhancing healing.

3. Graphene and Ferrocene Additions:

- The inclusion of graphene likely contributes to the high surface area, mechanical strength, and electrical conductivity, which could enhance the bioactivity and functional integration with bone tissue.
- Ferrocene's role may offer unique properties, such as improved biocompatibility and antibacterial characteristics, further supporting the composite's application in bone repair.

4. Biomedical Suitability:

- The interconnected pore structure, as indicated by the BJH analysis, facilitates nutrient and fluid exchange, promoting cell growth and adhesion. These properties are essential for the success of bone pin materials.

Property	**Value**
BET Surface Area (Multi-point)	105.6 m^2/g
Langmuir Surface Area	84.36 m^2/g
Total Pore Volume (<100 Å)	1.537e-01 cc/g
Average Pore Radius (BET)	41.75 Å (4.175 nm)
BJH Adsorption Mode Pore Radius	76.50 Å (7.65 nm)
BJH Desorption Mode Pore Radius	44.60 Å (4.46 nm)

Table 4.2-Summary of BET analysis

Conclusion

This composite demonstrates strong potential for use in orthopaedic applications, particularly as bone pins. Its high surface area and tailored porosity, combined with the synergistic properties of hydroxyapatite, graphene, and ferrocene, suggest it is well-suited for promoting bone healing and integration while resisting infection and wear.

5. Biocompatibility and Cytotoxicity Analysis

5.1 Biocompatibility analysis

Biocompatibility Analysis (MTT Assay on L929 Fibroblasts): This test assesses the viability and metabolic activity of normal fibroblast cells (L929 cell line) after exposure to the sample. The goal is to determine if the material is compatible with human cells, promoting their growth without causing harm.

Working Principle of the MTT Assay:

The MTT assay is based on the principle that viable cells are capable of converting a yellow water-soluble tetrazolium salt (MTT) into an insoluble, dark blue formazan product. The extent of this conversion correlates with the metabolic activity and viability of the cells. Here's a step-by-step overview of how it works:

1. ***Cell Seeding***: Cells are cultured in a 96-well plate and exposed to different concentrations of the test sample or drug.
2. ***MTT Addition***: After a set incubation period (usually 24 hours), MTT reagent is added to each well. Only metabolically active (live) cells are able to reduce MTT into formazan crystals.
3. ***Incubation***: The plate is incubated for 3–4 hours to allow the cells to reduce MTT into formazan.
4. ***Solubilization***: The formazan crystals are then solubilized with a solvent (such as DMSO) to release the formazan dye into the solution.
5. ***Measurement****:* The absorbance of the formazan solution is measured at a wavelength of 550 nm using a microplate reader. The intensity of the absorbance is directly proportional to the number of viable cells.

- **High Absorbance (or low inhibition)**: Indicates higher cell viability.
- **Low Absorbance (or high inhibition)**: Indicates a higher degree of cytotoxicity, meaning fewer live cells.

By comparing the absorbance values from the test samples with that of the control (untreated) group, the percentage of cell viability and cytotoxicity can be calculated.

The test was performed at Infinite Biotech Institute of Research And Analytics, Sangli Maharashtra, India.

Experimental procedure for biocompatibility

1. L929 Cells were incubated at a concentration of 1 × 104 cells/ml in culture medium for 24h at 37°C and 5% CO2.

2. Cells were seeded at a concentration (100µl) 104 cells/well) in 100µl culture medium and 20,40, 60, 80, 100 µg/ml of Samples into micro plates respectively (tissue culture grade, and 96 wells).

3. Control wells were incubated with DMSO (0.2% in PBS) and cell line. All samples were incubated in triplicate. Controls were maintained to determine the control cell survival and the percentage of live cells after culture.

4. Cell cultures were incubated for 24 h at 37°C and 5% CO2 in CO2 incubator.

5. After incubation, the medium was completely removed and Added 20µl of MTT reagent(5mg/ml PBS).

6. After addition of MTT, cells incubated for 4 hours at 37o C in CO2 incubator.

7. Observed the wells for formazan crystal formation under microscope. The yellowish MTT was reduced to dark coloured formazan by viable cells only.

8. After removing the medium completely. Added 200µl of DMSO (kept for 10min) and incubate at 37o C (wrapped with aluminium foil).

9. Triplicate samples were analyzed by measuring the absorbance of each sample by a microplate reader at a wavelength of 550 nm.

SR NO	SAMPLE CODE	Conc. (µg/ml)	OD			Mean	% Of Inhibition	% Of Viability	IC50 (µg/ml)
1	Control		1.532			-	-	-	-
2	Standard	**20**	1.305	1.304	1.303	**1.304**	**14.88%**	**85.12%**	
	Ethanol	**40**	0.820	0.824	0.820	**0.821**	**46.40%**	**53.6%**	
		60	0.762	0.760	0.762	**0.761**	**50.32%**	**49.68%**	**41.30**
		80	0.362	0.360	0.361	**0.361**	**76.43%**	**23.57%**	
		100	0.259	0.258	0.258	**0.258**	**83.15%**	**16.85%**	
3	ABS2-RT	**20**	1.372	1.370	1.372	**1.371**	**10.50%**	**89.49%**	
		40	1.346	1.345	1.346	**1.345**	**12.20%**	**87.79%**	
		60	1.291	1.292	1.291	**1.291**	**15.73%**	**84.26%**	**NE**
		80	1.274	1.275	1.274	**1.273**	**16.90%**	**83.09%**	
		100	1.260	1.261	1.260	**1.260**	**17.75%**	**82.24%**	

Table 5.1- Effect of nanocomposite against L929 cell lines.

Graphical data:

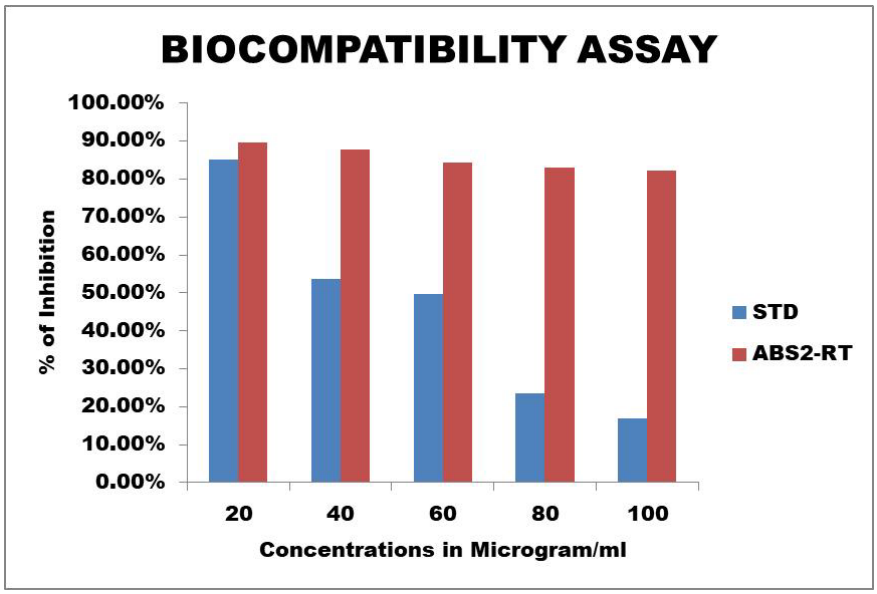

Figure 5.1-Graphical representation of biocompatibility at varying concentrations.

Conclusion:

At the different Concentrations most of the sample code shows the low percentage of inhibition and high percentage of cell viability against L929 Cell line as compared to standard drug 5FU. On the basis of percent of viability we can conclude that the most of the samples have compatibility nature.

6. Methodology of Bone Pin Formation Using Powder Metallurgy

6.1. Material Preparation

The HA composite, consisting of hydroxyapatite (HA), graphene, and ferrocene, is prepared by thoroughly mixing the components into a fine, uniform powder. This composite is chosen for its enhanced mechanical properties due to the incorporation of graphene and ferrocene.

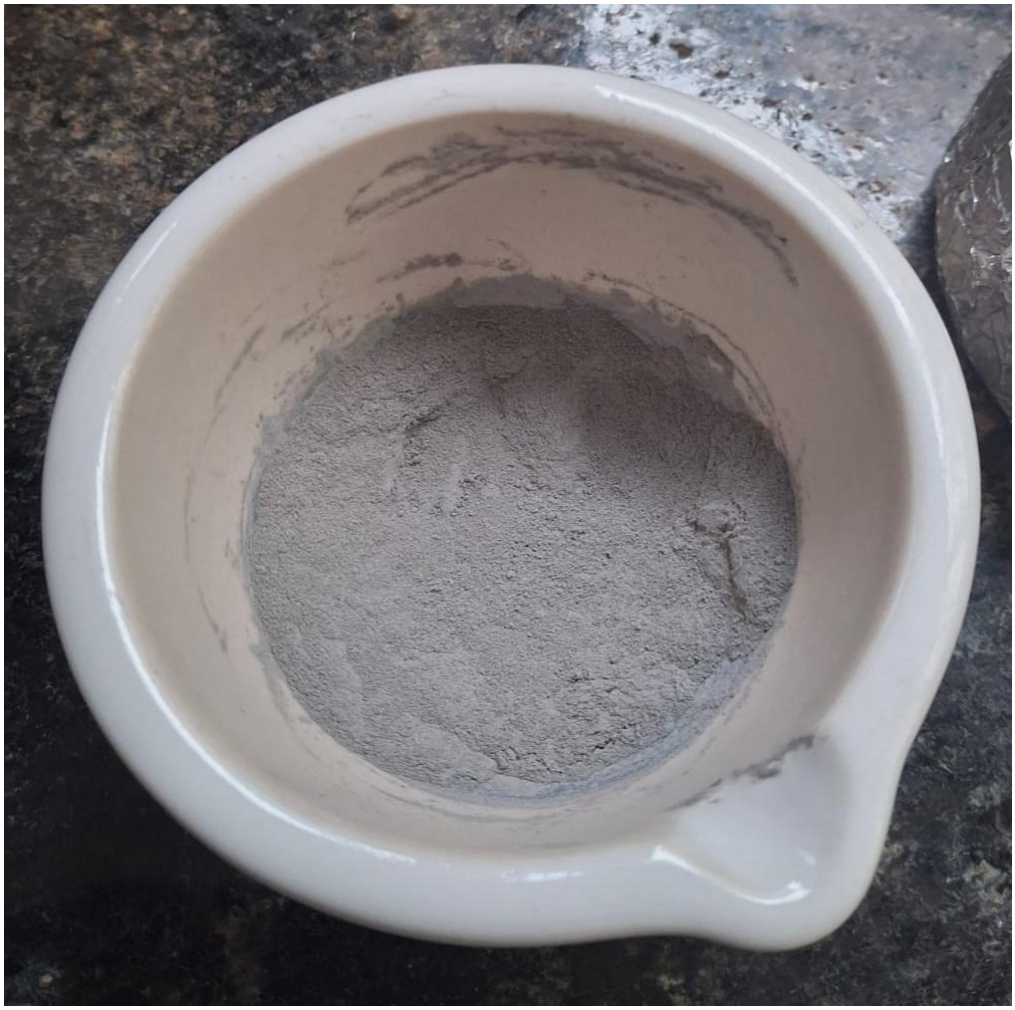

Figure 6.1- Nano composite powder.

6.2. Die Design and Setup

The bone pin is formed using a cylindrical die with the following dimensions:

Die Length: 6 cm

Die Diameter: 3 cm

Hole Diameter: 1 cm (for the formation of the pin)

The die is designed to withstand the applied pressure during compaction. One small screw is inserted at the base and removed at the end of the process, while a Universal Testing Machine (UTM) is used to apply pressure during the compaction of the HA composite powder.

6.3. Screw Specifications

Small Screw: The small screw, 3.75 cm in length (including a 2 cm head) and 1 cm in diameter, is used for compacting the powder inside the die. This screw is inserted at the base and removed at the end of the compaction process.

Large Screw: The large screw, 8 cm in length (including a 2 cm head) and 1 cm in diameter, is used to eject the compacted bone pin from the die after compaction.

Figure 6.2- Die and pin setup.

6.4. Compaction Process

1. ***Initial Loading:***

o The die is placed on a stable surface, and one small screw is inserted into one end of the die to securely block it.

o The prepared HA composite powder is filled into the die cavity up to a height of approximately 3–4 cm.

2. ***First Compaction (Using the UTM and Small Screw):***

o The second small screw is inserted into the open end of the die.

o The UTM is used to apply pressure to the die to compress the powder. The applied pressure is monitored and adjusted to ensure uniform compaction.

o The 2 cm head on the small screw ensures that pressure is evenly distributed during compaction.

3. ***Layering and Repeating the Process:***

o After the first layer is compacted, the small screw is removed from the compacted end of the die.

o Additional layers of HA composite powder are added, and the compaction process is repeated. The second small screw is inserted each time, and pressure is applied using the UTM until each layer is uniformly compacted.

o This process is repeated until the die is nearly full, leaving only 1 mm of space at the top for the final ejection of the bone pin.

6.5. Bone Pin Ejection

1. ***Using the Large Pin for Removal:***

o Once the die is fully compacted, both small screws are removed from the die.

o The large screw is inserted into the open end of the die and is tightened slowly to apply pressure and eject the compacted bone pin from the die cavity.

o The large screw is used carefully to ensure that the bone pin is removed without damage.

2. ***Cleaning and Inspection:***

o After the bone pin is ejected, it is inspected for any defects, such as cracks, surface irregularities, or incomplete compaction.

Figure 6.4-Bone pin after removal from Die

7. Mechanical Analysis.

7.1 Density analysis: -

Density analysis is essential for ensuring the nanocomposite bone pin meets structural, mechanical, and biocompatibility requirements. It validates the manufacturing process and ensures the implant's performance and safety in biomedical applications.

Structural Integrity: Ensures the pin is free of voids or cracks and confirms uniform compaction for reliable performance.

Mechanical Strength: Correlates density with strength and stiffness, ensuring the pin can bear physiological loads without failure.

Biocompatibility: Optimizes porosity for osseointegration while preventing excessive porosity that could weaken the pin.

Quality Control: Validates manufacturing consistency and identifies defects before use.

Natural Bone Mimicry: Ensures density compatibility with natural bone to avoid stress mismatch and promote integration.

Density of the bone pin was analysed by measuring the volume and the weight of the prepared bone pin

Volume-

Diameter of bone pin(d) - 1cm

Length of bone pin (l)– 2.5cm

Volume = $\pi(d/2)2l$

Volume = $\pi(0.5)$ 22.5

Volume =1.96375 cm2

Weight-

The weight was measured using sensitive weight balance.

Weight= 0.80631gm

Density-

Hence density can be calculated as

Density = Weight

Volume

Density = 0.80631/1.96375

Density = 0.4106 gm/cc

The natural density of bone lies between 0.95 gm/cc.

7.2 Finite Element Analysis:

Finite Element Analysis (FEA) is a powerful computational tool used to investigate the mechanical behaviour of nanocomposite materials, particularly at the nanoscale. This technique involves discretizing complex geometries, material properties, and interactions into smaller, finite elements to provide detailed insights into their structural and functional performance.

1. Modeling of Solid Cylinder.

The artificial bone pin was modeled as a solid cylindrical structure using ANSYS Workbench software to simulate its mechanical performance under physiological conditions. The geometry was chosen to resemble typical orthopaedic implants in size and functionality.
Specifications of the Model:
Diameter: 10 mm
Length: 30 mm

Steps in the Design Process:

1. Sketching the Base Geometry:

o A circle with a diameter of 10 mm was created in the XY plane as the cross-sectional profile of the cylinder.

o The circle was positioned at the origin for symmetry and ease of extrusion.

2. Extrusion:

o The sketched circle was extruded along the Z-axis to a length of 100 mm, forming a 3D cylindrical solid model.

o This step ensured uniform dimensions; representative of a typical bone pin used in orthopaedic implants.

3. Validation of Dimensions:

o The final model was inspected for any geometric inconsistencies to ensure precision in subsequent analyses.

o The dimensions were specifically chosen to replicate realistic orthopaedic bone pins while maintaining computational efficiency during simulation.

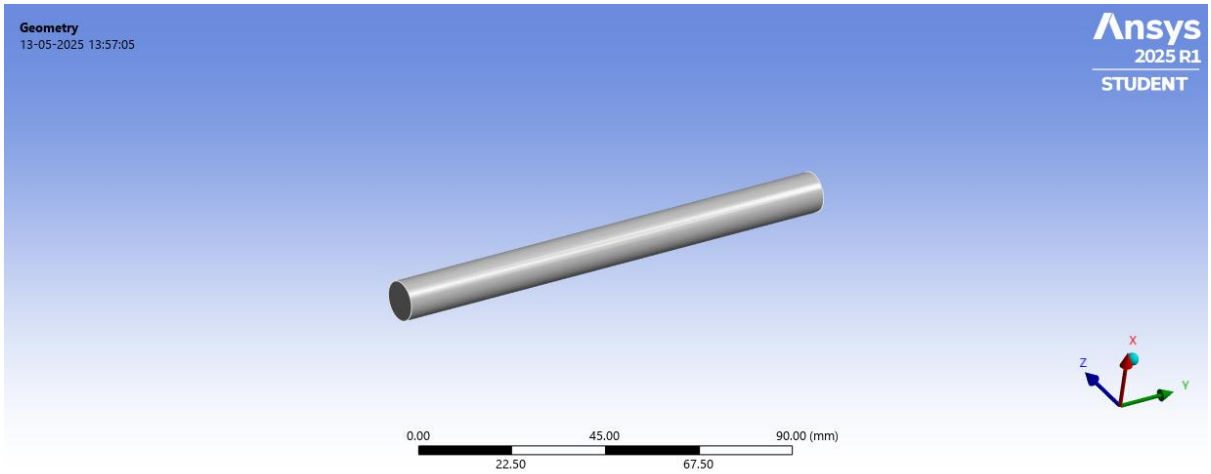

Figure 7.1 Extruded cylinder.

2. Meshing

Meshing is a critical step in finite element analysis, ensuring that the model is discretized into smaller elements for numerical computations.

Details of Meshing:

Nodes: 27,269

Elements: 6,496

A tetrahedral mesh type was used, which is well-suited for cylindrical geometries.

The element size was optimized to balance accuracy and computational time, with finer mesh density applied to regions expected to experience higher stress and deformation.

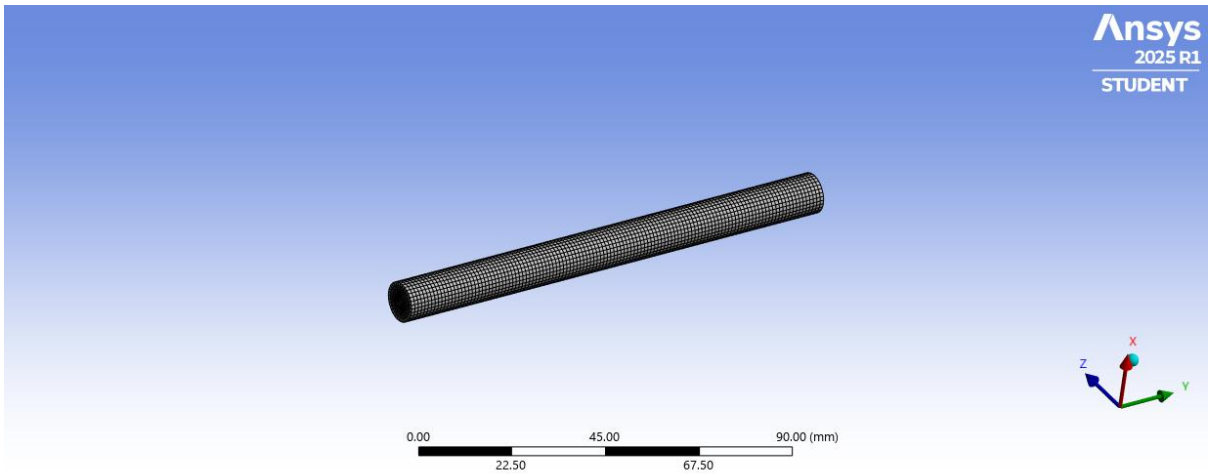

Figure 7.2- Meshed Cylinder.

3. Boundary Conditions

To simulate realistic loading conditions experienced by bone pins in the human body, the following boundary conditions were applied:

1. Fixed Support:

o One end of the cylinder was fixed to mimic its attachment to the bone or implant structure.

o This constraint restricted all translational and rotational movements at the fixed end.

2. Load Application:

o A compressive force of 750 Pa was applied uniformly across the opposite end of the cylinder.

o This load represents the stress generated by the body weight of a 75 kg individual during static activities like standing.

The boundary conditions were carefully chosen to reflect the primary compressive forces that bone pins encounter in clinical applications.

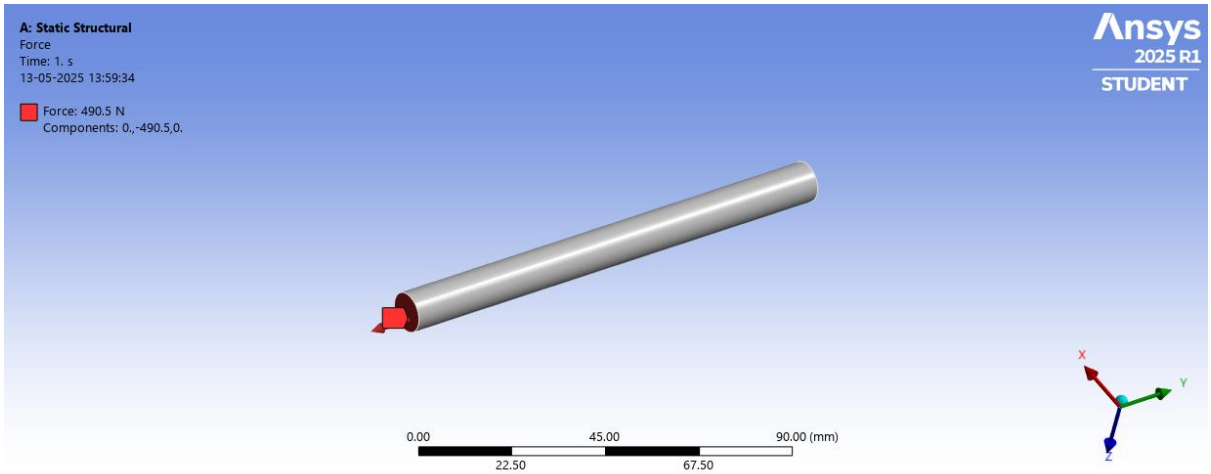

Figure 7.3- Mesh with Boundary conditions applied.

Observations: -

The simulation yielded critical insights into the bone pin's mechanical behaviour:

1. ***Directional Deformation:***

o The maximum deformation observed was 1.1898 mm at the free end of the cylinder.

o This deformation is well within acceptable limits for load-bearing orthopaedic applications, ensuring stability and functionality under physiological conditions.

2. ***Equivalent Stress Distribution:***

o **Maximum Stress:** 871 MPa, observed near the fixed support where stress concentration was highest.

o **Minimum Stress:** 541.89 MPa, recorded in regions away from the load application and support areas.

These stress values confirm the bone pin's ability to withstand physiological compressive loads without failure, highlighting its potential for orthopaedic applications.

4. Tensile Test

The tensile test was conducted to determine the material's ability to resist axial elongation under uniaxial tensile loads.

Maximum Load: 6.87 kN, the maximum force the material sustained before fracture.

Ultimate Tensile Strength (UTS): 0.092 N/mm², calculated by dividing the maximum load by the cross-sectional area.

Displacement at Ultimate Load: 13.85 mm, indicating the elongation of the specimen at maximum load.

Yield Load: 3.86 kN, the load at which the material transitioned from elastic deformation to plastic deformation.

Yield Stress: 0.054 N/mm², derived by dividing the yield load by the cross-sectional area.

The tensile test results reveal that the material demonstrates moderate ductility and strength, suitable for applications requiring some flexibility to match the mechanical behavior of bone.

Compressive Test

The compressive test analyzed the material's ability to withstand axial compressive loads without undergoing failure.

Maximum Load: 9.90 kN, the maximum compressive force the material endured before failure.

Compressive Strength: 81.2 MPa, determined by dividing the ultimate load by the cross-sectional area.

Displacement at Maximum Load: 5.62 mm, representing the deformation of the specimen at the point of failure.

Yield Load: 7.89 kN, the load at which permanent deformation initiated in the material.

Yield Stress: 68.4 MPa, calculated by dividing the yield load by the cross-sectional area.

The results show that the material exhibits significant compressive strength, making it ideal for load-bearing implants subjected to axial compressive forces.

7.3 Tribological Analysis:

Tribological characterization was conducted to evaluate the frictional and wear properties of the artificial bone pin material. A pin-on-disc tribometer was utilized to simulate sliding contact conditions similar to those experienced in joint and bone pin applications.

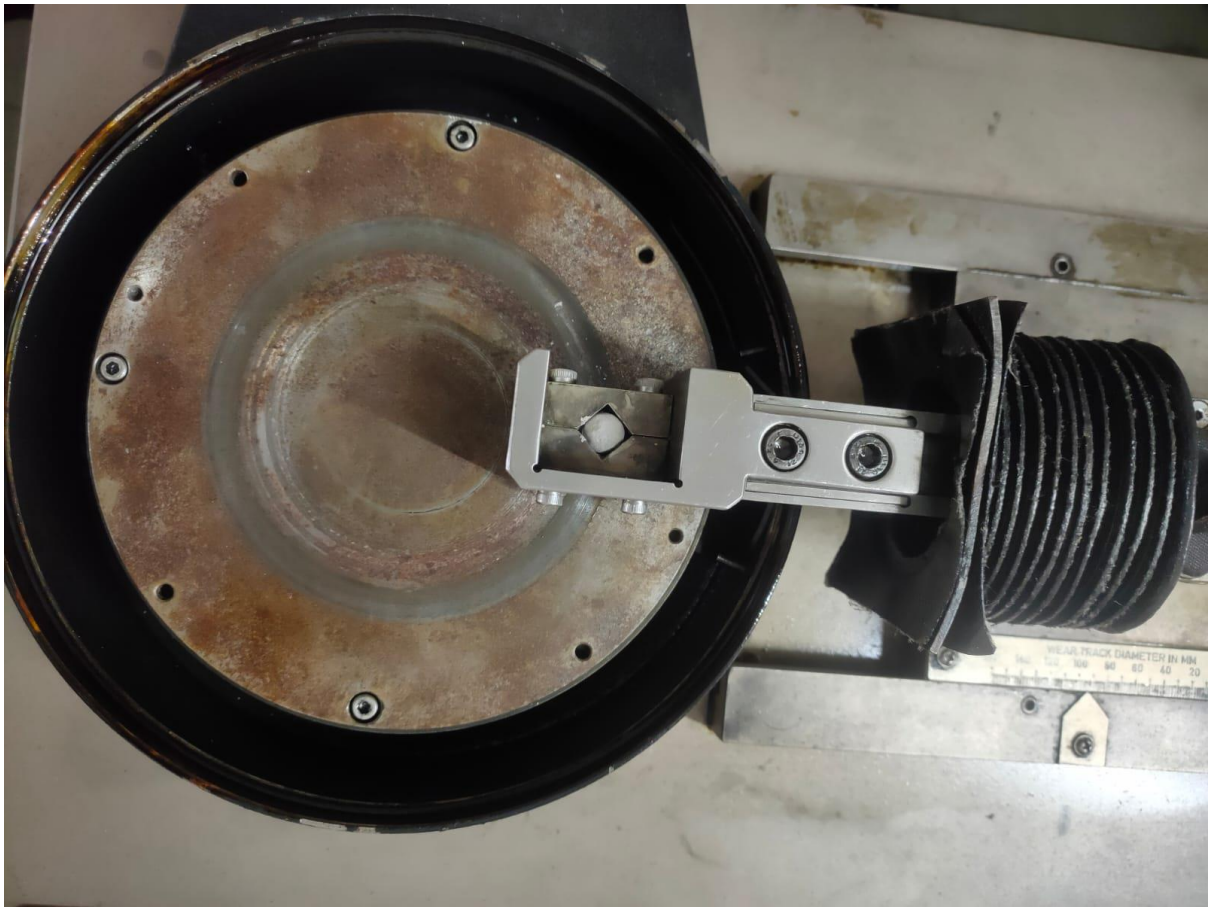

Figure 7.4-Test setup for tribological testing.

Experimental Setup and Procedure:

1. ***Specimen Preparation:***

o Pins were fabricated from the nanocomposite material (Sample 1) with a length of 30 mm and a diameter of 10 mm, ensuring compatibility with the tribometer's pin holder.

o The pins were polished to maintain uniform contact with the disc surface.

2. ***Pin-on-Disc Configuration:***

o **Track Diameter:** The disc was configured to maintain a constant track diameter of 70 mm, ensuring uniform sliding conditions.

o **Disc Material:** The disc was made of mild steel (MS), a common standard for tribological tests.

3. ***Operational Parameters:***

o **Speeds:** Sliding speeds of 50, 100, and 150 rpm were tested.

Loads: Normal loads of 0.5 kg, 1 kg, and 1.5 kg were applied to evaluate the material's response under varying contact pressures.

o **Lubricant:** Distilled water was used in submerged conditions to simulate a lubricated environment.

4. ***Data Acquisition:***

o The tribometer was equipped with a computerized data acquisition system to record real-time frictional force and wear data.

o Test durations were adjusted based on speed and load to ensure consistent wear conditions across all trials.

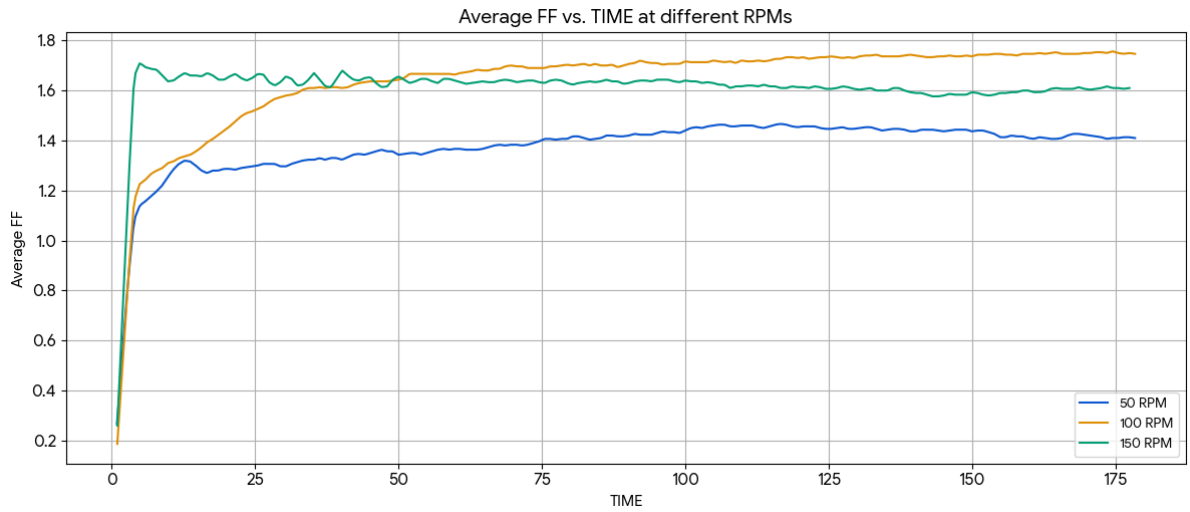

Figure 7.5- Wear, Frictional Force and COF charts of tribological testing

1. Wear vs. Time

Observations:

o The wear depth increases linearly during the initial stages (0–50 seconds), indicating a consistent wear rate.

o Peaks are observed at intervals (around 50–120 seconds and 160–220 seconds), which could be caused by external factors such as variations in material contact or surface imperfections.

o A sharp reduction in wear depth is seen at the end, suggesting a potential test reset or anomaly in the experimental setup.

Conclusion:

The material demonstrates a steady wear rate in the initial phase, suggesting good resistance to mild abrasive forces.

Peaks and fluctuations indicate dynamic material interactions, likely due to microstructure effects or debris.

2. Coefficient of Friction (COF) vs. Time

Observations:

o The COF begins at a high value (~1.0) and decreases over the initial 50 seconds, stabilizing around 0.8.

o Over time, the COF exhibits minor fluctuations, maintaining a relatively stable average (Mean = 0.765).

o Toward the end of the test (~280 seconds), there is a sudden increase followed by a sharp drop.

Conclusions

o The COF stabilizes at ~0.765, which is within an acceptable range for low-friction materials in load-bearing applications.

o The sudden fluctuation at the end may indicate reaching the material's tribological limit.

3. Frictional Force vs. Time

Observations:

o The frictional force starts at a lower value (~2.0 N) and steadily increases, stabilizing around 3.5 N after the initial 50 seconds.

o Fluctuations in force are minimal during the steady-state phase, indicating consistent sliding behaviour.

o A sharp rise in force is observed toward the end of the test (~280 seconds), followed by a sudden drop.

Conclusions

o The steady force during the middle phase is a positive indicator of the material's consistent performance under prolonged loading.

8. Result Analysis

8.1 Chemical and Structural Result Analysis.

1. Fourier Transform Infrared (FTIR) Spectroscopy

o Identified functional groups, confirming the integration of hydroxyapatite (OH^-, CO_3^{2-}, PO_4^{3-}) and graphene (C=C vibrations).

o Structural integrity was verified for individual components within the composite.

o Confirms chemical bonding and the successful integration of composite elements.

2. X-Ray Diffraction (XRD)

o Sharp peaks at 30°–35° confirm the crystalline structure of hydroxyapatite.

o Contributions from graphene (26°) and ferrocene were identified, indicating the multiphase nature of the composite.

o Provides evidence of high crystallinity and successful phase integration.

3. Transmission Electron Microscopy (TEM)

o Nanoparticles in the range of 20–60 nm.

o Layered graphene structures with hydroxyapatite and ferrocene incorporated.

o Demonstrates nanoscale uniformity and effective dispersion of components.

4. Energy-Dispersive X-ray Spectroscopy (EDX)

o High carbon content (graphene), calcium and phosphorus (hydroxyapatite), and iron (ferrocene) detected.

o Slight stoichiometric deviations in hydroxyapatite.

o Validates elemental contributions from all composite components.

5. Raman Spectroscopy

o Presence of D and G bands confirms graphene's structural integrity and defect levels.

o Phosphate group vibrations validate hydroxyapatite presence.

o Confirms interactions and structural retention of components in the composite.

6. Thermogravimetric Analysis/Differential Thermal Analysis (TGA/DTA)

o High stability with 95.48% mass retention up to 1000°C.

o Minor decomposition at ~465°C and ~495°C.

o Highlights the composite's suitability for high-temperature applications.

7. BET Surface Area Analysis

o Surface area: ~105.6 m^2/g.

o Mesoporosity (41–76 Å pore size).

o Indicates high porosity suitable for biomedical applications like drug delivery and cell growth.

8.2 Biocompatibility and Cytotoxicity Result Analysis.

1. Biocompatibility (L929 Fibroblast Cells)

o High cell viability was observed at all concentrations (20–100 μg/ml), with minimal inhibition of fibroblast growth.

o The composite is highly biocompatible, supporting the growth and activity of fibroblast cells critical for tissue regeneration.

2. Cytotoxicity (MCF10A Epithelial Cells)

o Low cytotoxicity with high cell viability across tested concentrations, showing minimal harmful effects on epithelial cells.

o The composite is non-toxic and safe for biomedical use, particularly in contact with human tissues.

8.3 Mechanical Result Analysis.

1. Density Analysis:

o Density is 0.4106 g/cc, which is lower than natural bone density (0.95 g/cc).

o The bone pin is lighter, which may affect its mechanical strength and compatibility. Potential optimization of compaction or material composition is needed.

2. Finite Element Analysis (FEA):

o Max deformation of 1.1898 mm is within acceptable limits, indicating good stability.

o **Stress Distribution:**

Max Stress: 871 MPa near fixed support shows significant stress concentration.

Min Stress: 541.89 MPa in unloaded regions demonstrates uniform load distribution.

o The pin can withstand physiological loads without failure, confirming its suitability for orthopaedic use.

Tensile Test:

o **Ultimate Tensile Strength (UTS):** 22.43 Mpa indicating moderate strength.

o **Displacement at UTS:** 2.5 mm, showing good elongation capacity.

o **Yield Stress:** 0.054 N/mm² reflects moderate ductility.

o The material offers flexibility, reducing the risk of brittleness-related failure.

Compressive Test:

o **Compressive Strength:** 63 MPa, showing excellent resistance to axial loads.

o **Yield Stress:** 52 MPa highlights strong load-bearing capabilities.

o The material is well-suited for applications requiring significant compressive strength, such as load-bearing implants.

3. Tribological Analysis:

o **Wear:** A consistent initial wear rate with fluctuations likely caused by microstructural factors or debris. Good resistance to mild abrasion.

o **COF (Coefficient of Friction):** Stabilizes at ~0.765, suitable for low-friction applications. Fluctuations may suggest reaching the material's limit under certain conditions.

o **Frictional Force:** Stable at ~3.5 N during steady-state, indicating consistent performance under prolonged sliding.

o The material exhibits favourable tribological behaviour with manageable wear and friction, making it reliable for joint or load-bearing applications.

9. Conclusion and Future Scope

9.1 Conclusion

9.1.1 Chemical and Structural Analysis conclusion:

The combined analyses establish that the composite material integrates its constituents effectively, retaining their structural and chemical properties while demonstrating excellent thermal stability and biocompatibility. Its high surface area and mesoporous structure make it promising for biomedical applications, particularly in bone repair and regeneration.

9.1.2 Biocompatibility and Cytotoxicity Analysis Conclusion

The composite material demonstrates excellent biocompatibility and low cytotoxicity, validating its potential for medical applications such as implants or bone repair.

9.1.3 Mechanical Analysis Conclusion

The nanocomposite material demonstrates promising mechanical and tribological properties, with some areas for optimization (e.g., density and microstructural uniformity). Its performance aligns well with orthopaedic implant requirements.

9.1.4 Overall Conclusion

The research on the nanocomposite bone pin material has demonstrated promising results across several critical areas. Chemical and structural analyses reveal that the material integrates its constituents effectively, maintaining their properties while offering excellent thermal stability and biocompatibility. This makes it a strong candidate for biomedical applications, particularly bone repair and regeneration.

Biocompatibility tests confirm the material's suitability for medical use, showing minimal cytotoxicity and an ability to support cellular growth, further enhancing its potential for implants and bone repair applications.

Mechanical and tribological analyses have highlighted the material's mechanical strength and wear resistance, key characteristics for orthopaedic implants. While certain aspects like density and microstructural uniformity may require optimization, the material's performance aligns well with the requirements for load-bearing implants.

In conclusion, this nanocomposite material shows significant promise for orthopaedic and biomedical applications, particularly for bone pins and implants. With further refinements in its structural properties and optimization for long-term durability, it holds strong potential for improving patient outcomes in bone repair and regeneration.

9.2 Future scope

This research provides a foundational understanding of the mechanical properties, material selection, and performance of bone pins. However, several areas offer opportunities for further investigation and development:

9.2.1 Material Enhancement and Testing:

Future work could focus on exploring new materials or composite formulations for bone pins. Incorporating bioactive components, optimizing porosity, and applying surface coatings could enhance the bone pin's strength, biocompatibility, and ability to integrate with bone tissue.

9.2.2 Advanced Finite Element Analysis (FEA):

Building on the current analysis, more complex simulations could be conducted to consider additional real-world factors such as temperature changes, fluid dynamics, and multi-axial loading conditions. This would provide a more comprehensive evaluation of the bone pin's performance under physiological conditions.

9.2.3 Tribological Long-Term Testing:

Further investigation into the wear and friction behavior of bone pin materials over extended periods is needed. Long-term tribological testing, including the effects of joint fluid and varying motion speeds, could provide deeper insights into the material's durability and reliability in the human body.

9.2.4 Personalized Implant Design:

Advancements in 3D printing and computational modeling could lead to the creation of customized bone pins tailored to individual patients. Personalized implants would ensure better fit and functionality, potentially improving patient outcomes.

9.2.5 Prototype Development and Clinical Testing:

The development of physical prototypes using additive manufacturing techniques could be pursued. Clinical trials, initially starting with animal models, would provide real-world data on the biological response to the bone pins and validate their performance under realistic conditions.

9.2.6 Improved Manufacturing Processes:

Exploring more efficient and scalable manufacturing methods, such as advanced 3D printing or injection molding, could improve the cost-effectiveness and consistency of producing bone pins at a larger scale, making them more accessible for clinical use.

References

[1] Sadat-Shojai, M., Khorasani, M.-T., Dinpanah-Khoshdargi, E., Jamshidi, A. (2013). Synthesis methods for nanosized hydroxyapatite with diverse structures. Acta Biomaterialia, 9(8), 7591?7621.

https://doi.org/10.1016/j.actbio.2013.04.012

[2] Sadat-Shojai, M., Khorasani, M.-T., Dinpanah-Khoshdargi, E., Jamshidi, A. (2013). Hydroxyapatite nanoparticles: A review of synthesis, properties, and applications. Biomaterials, 34(28), 6679?6711.

https://doi.org/10.1016/j.biomaterials.2013.05.036

[3] Dorozhkin, S.V. (2010). Bioceramics of calcium orthophosphates. Biomaterials, 31(7), 1465?1485. https://doi.org/10.1016/j.biomaterials.2009.11.050

[4] Dorozhkin, S.V. (2009). Calcium orthophosphates in nature, biology and medicine. Materials, 2(2), 399?498. https://doi.org/10.3390/ma2020399

[5] Vallet-Regi, M., Gonzalez-Calbet, J.M. (2004). Calcium phosphates as substitutionof bone tissues. Progress in Solid State Chemistry, 32(1‑2), 1‑31. https://doi.org/10.1016/j.progsolidstchem.2004.07.001

[6] Kokubo, T., Kim, H.M., Kawashita, M. (2003). Novel bioactive materials with different mechanical properties. Biomaterials, 24(13), 2161?2175. https://doi.org/10.1016/S0142-9612(03)00044-9

[7] Garvie, R.C., Hannink, R.H.J., Pascoe, R.T. (1975). Ceramic steel? Nature, 258, 703?704. https://doi.org/10.1038/258703a0

[8] Garvie, R.C. (1978). Stabilization of the tetragonal structure in zirconia microcrystals. Journal of Physical Chemistry, 82(2), 218?224. https://doi.org/10.1021/j100491a016

[9] Garvie, R.C. (1965). Metastable tetragonal zirconia. Journal of Physical Chemistry, 69(4), 1238?1243. https://doi.org/10.1021/j100888a024

[10] Hannink, R.H.J., Kelly, P.M., Muddle, B.C. (2000). Transformation toughening in zirconia-containing ceramics. Journal of the American Ceramic Society, 83(3),

461?487. https://doi.org/10.1111/j.1151-2916.2000.tb01221.x

[11] Chevalier, J., Gremillard, L., Virkar, A.V., Clarke, D.R. (2009). The tetragonal?monoclinic transformation in zirconia: Lessons learned and future trends. Journal of the American Ceramic Society, 92(9), 1901?1920. https://doi.org/10.1111/j.1551-2916.2009.03278.x

[12] Chevalier, J., Gremillard, L. (2009). Ceramics for medical applications: A picture for the next 20 years. Journal of the European Ceramic Society, 29(7), 1245?1255. https://doi.org/10.1016/j.jeurceramsoc.2008.08.025

[13] Kelly, J.R., Denry, I. (2008). Stabilized zirconia as a structural ceramic: An overview. Dental Materials, 24(3), 289?298. https://doi.org/10.1016/j.dental.2007.05.005

[14] Ramesh, S., Tan, C.Y., Bhaduri, S.B., Teng, W.D. (2007). Processing and properties of nanocrystalline hydroxyapatite derived from wet-chemicalsynthesis. Journal of Materials Processing Technology, 206(1?3), 221?230.

https://doi.org/10.1016/j.jmatprotec.2007.12.019

[15] Balasubramanian, P., et al. (2014). Zirconia?alumina composites for orthopaedic applications. Journal of the European Ceramic Society, 34(12), 2915?2926.

https://doi.org/10.1016/j.jeurceramsoc.2014.04.013

[16] Anselme, K. (2000). Osteoblast adhesion on biomaterials. Biomaterials, 21(7), 667?681. https://doi.org/10.1016/S0142-9612(99)00242-2

[17] Anselme, K., Bigerelle, M. (2005). Effect of surface topography on cell?biomaterial interactions. Journal of Biomedical Materials Research Part A, 75A(1), 89?97.

https://doi.org/10.1002/jbm.a.30563

[18] Anselme, K., et al. (2010). The interaction of cells and bacteria with surfaces] structured at the nanometre scale. Acta Biomaterialia, 6(10), 3824?3846.

https://doi.org/10.1016/j.actbio.2010.04.001

[19] Webster, T.J., Ergun, C., Doremus, R.H., Siegel, R.W., Bizios, R. (2000).] Enhanced osteoclast-like cell functions on nanophase ceramics. Biomaterials,

22(11), 1327?1333. https://doi.org/10.1016/S0142-9612(00)00275-2

[20] Webster, T.J., Ergun, C., Doremus, R.H., Siegel, R.W., Bizios, R. (2000). Specific proteins mediate enhanced osteoblast adhesion on nanophase ceramics. Journal of Biomedical Materials Research, 51(3), 475?483. https://doi.org/10.1002/1097- 4636(20000905)51:3!475::AID-JBM19.3.0.CO;2-S

[21] Nayak, A.K. (2010). Hydroxyapatite synthesis methodologies: An overview. International Journal of ChemTech Research, 2(2), 903?907.

[22] Wang, P., Li, C., Gong, H., Jiang, X., Wang, H., Li, K. (2010). Effects of synthesis conditions on the morphology of hydroxyapatite nanoparticles produced by wet chemical process. Powder Technology, 203(2), 315?321. https://doi.org/10.1016/j.powtec.2010.05.012

[23] Ren, F., Leng, Y., Xin, R., Ge, X. (2010). Synthesis, characterization and abinitio simulation of magnesium-substituted hydroxyapatite. Acta Biomaterialia,

6(7), 2787?2796. https://doi.org/10.1016/j.actbio.2010.01.042

[24] Eliaz, N., Metoki, N. (2017). Calcium phosphate bioceramics: A review of their history, structure, properties, coating technologies and biomedical applications.

Materials, 10(4), 334. https://doi.org/10.3390/ma10040334

[25] Uskokovi?, V. (2015). Insights into morphological nature of precipitation of calcium phosphates. Materials Science and Engineering: C, 55, 14?28.

https://doi.org/10.1016/j.msec.2015.04.020

[26] Bose, S., Tarafder, S. (2012). Calcium phosphate ceramic systems in growth factor and drug delivery for bone tissue engineering: A review. Acta Biomaterialia, 8(4),

1401?1421. https://doi.org/10.1016/j.actbio.2011.11.017

[27] Dorozhkin, S.V. (2011). Calcium orthophosphates in nature, biology and medicine. Materials, 4(6), 1057?1111. https://doi.org/10.3390/ma4061057

[28] Dorozhkin, S.V. (2012). Biphasic, triphasic and multiphasic calcium orthophosphates. Acta Biomaterialia, 8(3), 963?977.

https://doi.org/10.1016/j.actbio.2011.09.003

[29] Wu, V.M., Uskokovi?, V. (2015). Is there a relationship between solubility and resorbability of different calcium phosphate phases in vitro? Biochimicaet Biophysica Acta (BBA) ? General Subjects, 1850(8), 1648?1658.

https://doi.org/10.1016/j.bbagen.2015.04.009

[30] Dorozhkin, S.V. (2013). Calcium orthophosphate-based bioceramics. Materials, 6(9), 3840?3942. https://doi.org/10.3390/ma6093840

[31] Webster, T.J., Siegel, R.W., Bizios, R. (1999). Osteoblast adhesion on nanophase ceramics. Biomaterials, 20(13), 1221?1227. https://doi.org/10.1016/S0142- 9612(99)00020-4

[32] Shi, Z., Huang, X., Cai, Y., Tang, R., Yang, D. (2009). Size effect of hydroxyapatite nanoparticles on proliferation and apoptosis of osteoblast-like cells. Acta

Biomaterialia, 5(1), 338?345. https://doi.org/10.1016/j.actbio.2008.07.023

[33] Cai, Y., et al. (2007). Role of hydroxyapatite nanoparticle size in bone cell proliferation. Journal of Materials Chemistry, 17(36), 3780?3787. https://doi.org/10.1039/B705129H

[34] Boanini, E., Gazzano, M., Bigi, A. (2010). Ionic substitutions in calcium phosphates synthesized at low temperature. Acta Biomaterialia, 6(6), 1882?1894.

https://doi.org/10.1016/j.actbio.2009.12.041

[35] Dey, A., et al. (2010). The role of prenucleation clusters in surfaceinduced calcium phosphate crystallization. Nature Materials, 9, 1010?1014.

https://doi.org/10.1038/nmat2900

[36] Dorozhkin, S.V. (2009). Calcium orthophosphates in dentistry. Journal of Materials Science: Materials in Medicine, 20(4), 819?837. https://doi.org/10.1007/s10856-008-3639-7

[37] Suchanek, W., Yoshimura, M. (1998). Processing and properties of hydroxyapatite-based biomaterials for use as hard tissue replacement implants. Journal of Materials Research, 13(1), 94?117. https://doi.org/10.1557/JMR.1998.0016

[38] Sopyan, I., Mel, M., Ramesh, S., Khalid, K.A. (2007). Porous hydroxyapatite for artificial bone applications. Science and Technology of Advanced Materials,

8(1?2), 116?123. https://doi.org/10.1016/j.stam.2006.11.017

[39] Legeros, R.Z. (2008). Calcium phosphate-based osteoinductive materials. Chemical Reviews, 108(11), 4742?4753. https://doi.org/10.1021/cr800427g

[40] Dorozhkin, S.V. (2010). Bioceramics of calcium orthophosphates. Biomaterials, 31(7), 1465?1485. https://doi.org/10.1016/j.biomaterials.2009.11.050

[41] Raynaud, S., Champion, E., Bernache-Assollant, D., Thomas, P. (2002). Calcium phosphate apatites with variable Ca/P atomic ratio I. Synthesis, characterization and thermal stability of powders. Biomaterials, 23(4), 1065?1072.

https://doi.org/10.1016/S0142-9612(01)00218-6

[42] Shannon, R.D. (1976). Revised effective ionic radii and systematic studies of interatomic distances in halides and chalcogenides. Acta Crystallographica Section A,

32(5), 751?767. https://doi.org/10.1107/S0567739476001551

[43] Pan, H.H., et al. (2007). Nucleation of amorphous calcium phosphate on negatively charged surfaces involves a two-step mechanism. Journal of Physical

Chemistry C, 111(28), 10219?10225. https://doi.org/10.1021/jp0722405

[44] Gibson, I.R., Bonfield, W. (2002). Novel synthesis and characterization of an AB-type carbonate-substituted hydroxyapatite. Journal of Biomedical Materials Research, 59(4), 697?708. https://doi.org/10.1002/jbm.10044

[45] Kim, H.W., Koh, Y.H., Kong, Y.M., Kang, J.G., Kim, H.E. (2004). Strontium substituted calcium phosphate biphasic ceramics for bone tissue engineering. Biomaterials, 25(17), 3403?3411. https://doi.org/10.1016/j.biomaterials.2003.09.048

[46] Bigi, A., Boanini, E., Gazzano, M. (2007). Strontium-substituted hydroxyapatite nanocrystals. Inorganic Chemistry, 46(15), 6200?6206. https://doi.org/10.1021/ic700426j

[47] Camire, C.L., et al. (2006). In vivo evaluation of injectable calcium phosphate cement with biodegradable fibers. Journal of Biomedical Materials Research Part B: Applied Biomaterials, 76B(2), 424‑431. https://doi.org/10.1002/jbm.b.30398

[48] Elliott, J.C. (1994). Structure and chemistry of the apatites and other calcium orthophosphates. Elsevier Science.

Conference Certificate

CERTIFICATE

RSP CONFERENCE HUB

Of Participation

This Certificate is Presented To

Mr. Suyog. Balavant. Sutar

Design Engineering, Rajarambapu Institute of Technology, Shivaji University, Sakharale, Maharashtra, India

For attending and giving an oral presentation on the paper entitled

Mechanical Evaluation of a Graphene–Zirconia Nanocomposite Bone Pin under Simulated Physiological Loads

at the ***"Second International Conference on Recent Trends in Science, Technology and Management (ICRTSTM) 2025"*** *- Jointly Organized by Bharati Vidyapeeth's College of Engineering for Women (BVCOEW), Pune, Maharashtra, India & RSP Conference hub, Coimbatore, Tamil Nadu, India on* ***30th June and 1st July, 2025.***

Prof. Dr. Ketaki A. Malgi	***Prof. Dr.Vijaya R Pawar,***	***Prof. Dr. Pradeep V. Jadhav***
Co- Convener-ICRTSTM 2025 & Associate Professor, BVCOEW, Pune	*Co- Convener-ICRTSTM-2025 & Associate Professor, BVCOEW, Pune*	*Convener-ICRTSTM-2025 & Principal- BVCOEW, Pune*

BVCOEW & RSP ICRTSTM 2025-306

Scopus Index Journal Paper

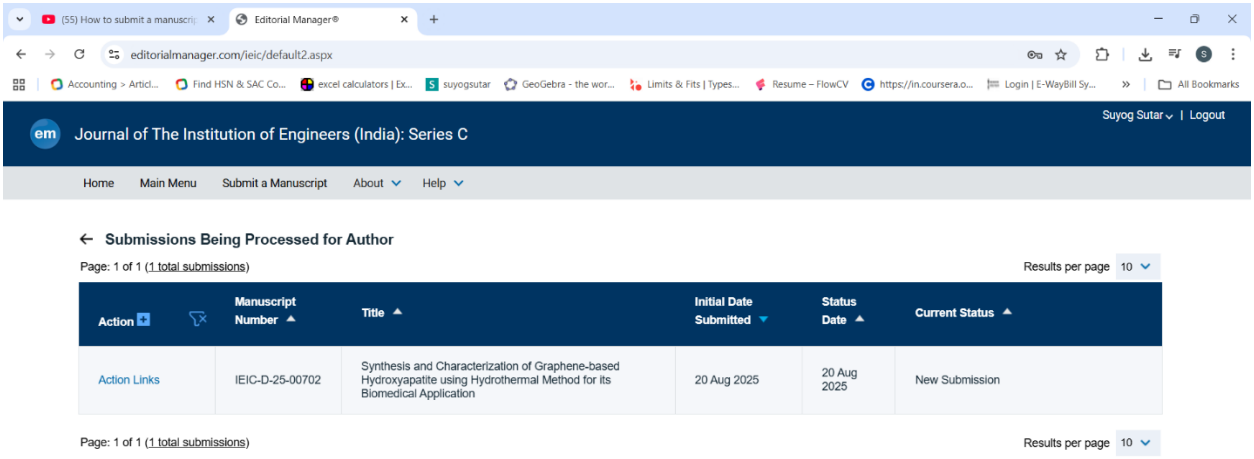

Latex Certificate

K. E. Society's

Rajarambapu Institute of Technology,

Rajaramnagar

An Autonomous Institute

SYNOPSIS OF M. TECH DISSERTATION

1. Name of Program	:	M. Tech. (Mechanical Design)
2. Name of student	:	Sutar Suyog Balavant
3. Enrollment No.	:	2321007
4. Date of registration	:	August 2023
5. Name of guide	:	Dr. S. R. Patil
6. Proposed title	:	**"Synthesis and Characterization of Graphene based hydroxyapatite nanocomposite by hydrothermal method for its biomedical application"**

7. Relevance:

Bone tissue loss due to trauma, surgery, or disease poses a significant medical challenge. Common treatments include autografts, allografts, xenografts, and synthetic grafts, each with benefits and limitations. Autografts involve tissue transfer within the same individual, while allografts use tissue from another human, and xenografts involve tissue from animals. Synthetic bone grafts, gaining popularity, offer advantages such as availability, sterility, cost-effectiveness, and reduced risk of rejection or infection. Artificial bones or joints can be implanted to restore structure and support regeneration. Their effectiveness depends on their composition, structure, and properties, offering a promising solution for bone repair and regeneration.

8.1 Present theories and practices: -

Patil S. R. et al. [1]

Investigated synthesis of Hydroxyapatite Polymethyl methacrylate Zirconia (Hap-PMMA-ZrO2) composite by using powder metallurgy technique. They have characterize mechanical, morphological, in vitro biocompatibility and tribological properties were characterized by universal testing machine, micro vickers hardness tester, high resolution transmission electron microscope (HR TEM), MTT assay and pin on disc setup of novel biocomopsite material. Hap-PMMA-ZrO2 scaffold displayed good biocompatibility and other properties.

Andrea Papait [2]

Graphene oxide (GO) is a promising nanomaterial for biomedical applications like bioimaging and drug delivery. This study explores how GO affects immune cell function when integrated into PLGA scaffolds. High GO levels reduce the viability of PBMCs and impair T cell activation and differentiation. GO minimally impacts resting monocytes but significantly affects monocyte maturation into M1 and M2 macrophages. This research highlights the importance of optimizing GO-to-PLGA ratios for safe biomaterial design, addressing concerns about immune responses and advancing GO-based clinical applications.

Shanmuga Priya Mohanaraman [3]

Graphene quantum dots (GQDs) are carbon nanomaterials known for their optical properties, engineered structures, and photostability. They are biocompatible, low in toxicity, hydrophilic, and have functionalized surfaces suitable for biological applications. GQDs emit various colors under UV light, with red light offering deep tissue penetration, cell imaging, and drug delivery benefits, making them ideal for photodynamic therapy. This review covers synthesis methods for red fluorescence GQDs (RF-GQDs), analyzes spectral characterization techniques, examines red emission mechanisms, and explores their biological applications and challenges, highlighting potential clinical and industrial uses.

Zobia Ayreen [4]

Advancements in nanotechnology have highlighted the potential of graphene oxide nanoparticles (GONP) due to their unique properties, but concerns about their immunotoxic effects have emerged. This review examines their interactions with biological systems, including human blood, immune cells, cancer cell lines, and in vivo models like mice and

zebrafish, revealing effects such as inflammation, immunosuppression, hypersensitivity, and cytotoxicity. It provides insights for researchers and policymakers to harness GONP's benefits while addressing health and environmental risks.

Rebecca Goodrum [5]

Graphene's exceptional properties, such as high conductivity and elasticity, make it ideal for biomedical applications like biosensing and drug delivery. This review highlights recent advances in green synthesis of graphene-based nanomaterials, focusing on top-down and bottom-up approaches. Applications in optical and electrochemical biosensors are explored, emphasizing their enhanced sensitivity for detecting biomolecules and cells. The benefits, challenges, and future directions of graphene-based biosensors are summarized, comparing their performance with conventional techniques.

Safeena Zafar [6]

Antimicrobial resistance necessitates new agents to protect health. Graphene and its derivatives, decorated with inorganic nanoparticles like FeO/NiO, show promising antibacterial and antifungal properties. Synthesized via a wet chemical method, these nanocomposites were analyzed using XRD, IR, SEM, and more. FeO/NiO/N-GO showed moderate antibacterial activity (MIC: 12.5 µg/mL), while FeO/NiO and FeO/NiO/S-GO exhibited strong antifungal effects. Their antioxidant, cytotoxic, and hemolytic potentials were also evaluated, with all showing significant activity. These findings support their potential in pharmaceutical and biomedical applications.

Shramila Yadav [7]

To promote sustainability, advanced systems with controlled performance are essential for biomedical, environmental, and energy applications. While graphene-based nanomaterials are well-studied, emerging 2D materials like TMDs, TMOs, MXenes, Xenes, and MOFs remain underexplored for next-gen biomedical uses. This review critically examines their roles in drug delivery, cancer therapy, tissue engineering, and biosensing, highlighting the need for better control over their shape, size, and properties. It fills a gap in the literature by providing a comprehensive analysis of these materials, offering valuable insights for researchers aiming to develop adaptable, high-performance 2D material-based applications.

8.2 Literature gap:

Mostly researcher mentioned the materials that is titanium alloy, stainless steel alloys and ceramics but the main problem with this material is they are stiffer than bone tissue may lead to mechanical mismatch problems (e.g., stress shielding) between the implant and the adjacent bone tissue.

The materials that is titanium alloys, steel alloys and zinc alloys which produce toxic cells when contact with blood i.e. use of bio-composite is needed.

8.3 Problem Statement:

In the field of health science for repair, replacement, and regeneration of bones the materials used presently are steels and other alloys. But the main problem encountered is; these materials produce toxic cells and compounds which are harmful and having number of disadvantages during repair and replacement work. In order to overcome these problems, there is need to development of material with proper mechanical properties without affecting biocompatibility.

8.4 Objectives:

1. To identify and select nanocomposite that exhibits the biocompatible properties.
2. To develop artificial bone pin using proposed nanocomposite material.
3. To synthesize nanocomposite by hydrothermal chemical method and characterize it.
4. To investigate mechanical properties of developed artificial bone pin by computational and experimental methods.
5. To check the biocompatibility of artificial bone pin material.

a. Proposed Work:

Phase I: Literature Survey

- Study will be done using extensive literature survey.
- Refer the journals and research papers on presents existing and relevant literature on material selection for artificial bone pin development.

Phase II: Selection and Synthesis

- Selection of different composites of graphene based nano composites
- Synthesis of selected composites using hydrothermal chemical method.
- Characterization of synthesized material using XRD, TEM, IR, EDX, etc.

Phase III: Characterization of artificial bone pin

- Manufacturing of artificial bone pin using suitable manufacturing process.
- Characterization of developed artificial bone will be carried out computationally and experimentally. The methodology will be followed for measurement of biocompatibility, tensile strength, compressive strength, hardness, coefficient of friction.

Phase IV: Modeling

- Analysis of the artificial bone pin using suitable software.

Phase V: Validation and Report Writing

- Validation of results by comparing the results between artificial and natural human bone and report writing.

8.5 Proposed Plan

Sr. No	Activity/month	Aug 2024	Sep 2024	Oct 2024	Nov 2024	Dec 2024	Jan 2025	Feb 2025	March 2025	April 2025	May 2025	June 2025
1	Literature Review											
2	Synthesis of proposed nono composite											
3	Characterization of developed artificial bone pin											
4	Validation of results by comparing the results between artificial and natural human bone pin											
6	Preparation of manuscript for journal and conferences											
7	Submission of Report											

8.9 Facilities Available

- Tribology Laboratory, Material Science Laboratory, Chemical Laboratory

Dept. of Mechanical Engg. RIT APPROVED COPY of Synopsis M. Tech Mechanical Design

Date : 24/09/2024

Place : RIT Rajaramnagar

Sutar Suyog Balavant
(Student)

Dr. S. R. Patil
Guide,
Mech. Engg. Dept.
R.I.T. Rajaramnagar

Dr. S. S. Gawade
Head of Program,
P. G. Mech. Design
R.I.T. Rajaramnagar

Dr. S. B. Kumbhar
Head Of Dept.,
Mech. Engg. Dept.
R.I.T. Rajaramnagar

nanocomposites for tissue engineering: a review." Polymer Degradation and Stability Vol. 95(2010): pp 2126–2146.

[16] Kharaziha, M., Fathi, M.H., Edris, H. "Effects of surface modification on the mechanical and structural properties of nanofibrous poly(epsilon-caprolactone)/forsterite scaffold for tissue engineering applications." Materials Science and Engineering and Materials for Biological Applications Vol.33 (2013): pp 4512–4519.

[17] Baro V J, Bonnevie E D, Lai X, Price C, Burris D L, Wang L. "Functional characterization of normal and degraded bovine meniscus: Rate-dependent indentation and friction studies." Bone Vol. 51 (2012): pp 232–240

[18] Dowson D. Modes of lubrication in human joints. "In Proceedings of the Institution of Mechanical Engineers" (1966): pp 45–54.

[19] Graindorge S, Ferrandez W, Jin Z M, Fisher J, Ingham E, Grant C, Twigg P. "Biphasic surface amorphous layer lubrication of articular cartilage." Medical Engineering and Physics Vol. 27(10) (2005): pp 836–844.

[20] Hills B A."Graphite-like lubrication of mesothelium by oligolamellar pleural surfactant." J Appl Physiol Vol.73(3) (1992): pp 1034–1039.

Plagiarism Checker X - Report

Originality Assessment

2%

Overall Similarity

Date: Aug 24, 2025 (10:54 PM)
Matches: 299 / 15416 words
Sources: 14

Remarks: Low similarity detected, consider making necessary changes if needed.

Verify Report:
Scan this QR Code

v 9.0.4 - WML 4
FILE - THESIS PHASE IV REPORT.PDF

Synthesis and Characterization of Graphene based hydroxyapatite nanocomposite by hydrothermal method for its biomedical application

by SUTAR SUYOG BALAVANT

General metrics

95,113	13,584	1110	54 min 20 sec	1 hr 44 min
characters	words	sentences	reading time	speaking time

Score

This text scores better than 91% of all texts checked by Grammarly

Writing Issues

378	110	268
Issues left	Critical	Advanced

Writing Issues

112	**Correctness**	
4	Improper formatting	
12	Confused words	
40	Determiner use (a/an/the/this, etc.)	
3	Faulty subject-verb agreement	

2	Pronoun use	
2	Wrong or missing prepositions	
17	Incorrect punctuation	
6	Misspelled words	
9	Comma misuse within clauses	
6	Incorrect verb forms	
9	Incorrect phrasing	
2	Closing punctuation	

3 Clarity

3	Wordy sentences	

Unique Words

Measures vocabulary diversity by calculating the percentage of words used only once in your document

16%

unique words

Rare Words

Measures depth of vocabulary by identifying words that are not among the 5,000 most common English words.

53%

rare words

Word Length

Measures average word length

5.6

characters per word

Sentence Length

Measures average sentence length

12.2

words per sentence

VITAE (CV)

Name : Mr. Suyog B. Sutar

Email : suyogbsutar@gmail.com

Phone : 8551877040

DOB : 30 Aug 1999

Program Name : Mechanical Engineering

Mr. Suyog B. Sutar completed his Diploma and BE in Mechanical Engineering in Kolhapur, and M.Tech in Mechanical Design Engineering at Rajarambapu Institute of Technology, Sangli. He has over 3.9 years of experience in new product design and casting development. Skilled in CAD modeling (SolidWorks, UG-NX, AutoCAD), GD&T, CAE analysis (Ansys), mold design, and product improvement. He currently works at Suyog Pattern, handling foundry component design and engineering changes. Suyog holds certifications in AutoCAD, Ansys, SolidWorks, UG NX/Solidedge, and is fluent in English, Hindi, and Marathi.